CO_2 Photocatalytic Reduction to Fuels

by:

Alejandro Castañeda Flores

A Thesis Submitted in Partial Fulfillment
of the Requirements for the Degree of Master of Science

Approved April 2014 by the
Graduate Supervisory Committee:

Jean M. Andino, Chair
Erica Forzani
César Torres

ARIZONA STATE UNIVERSITY
May 2014

ABSTRACT

A new photocatalytic material was synthesized to investigate its performance for the photoreduction of carbon dioxide (CO_2) in the presence of water vapor (H_2O) to valuable products such as carbon monoxide (CO) and methane (CH_4). The performance was studied using a gas chromatograph (GC) with a flame ionization detector (FID) and a thermal conductivity detector (TCD). The new photocatalytic material was an ionic liquid functionalized reduced graphite oxide (IL-RGO (high conductive surface))-TiO_2 (photocatalyst) nanocomposite. Brunauer-Emmett-Teller (BET), X-ray photoelectron spectroscopy (XPS), Raman spectroscopy, and UV-vis absorption spectroscopy techniques were employed to characterize the new catalyst. In the series of experiments performed, the nanocomposite material was confined in a UV-quartz batch reactor, exposed to CO_2 and H_2O and illuminated by UV light. The primary product formed was CO with a maximum production ranging from 0.18-1.02 $\mu mol(g_{catalyst}\text{-}hour)^{-1}$ for TiO_2 and 0.41-1.41 $\mu mol(g_{catalyst}\text{-}hour)^{-1}$ for IL-RGO-TiO_2. A trace amount of CH_4 was also formed with its maximum ranging from 0.009-0.01 $\mu mol(g_{catalyst}\text{-}hour)^{-1}$ for TiO_2 and 0.01-0.04 $\mu mol(g_{catalyst}\text{-}hour)^{-1}$ for IL-RGO-TiO_2. A series of background experiments were conducted and results showed that; (a) the use of a ionic liquid functionalized reduced graphite oxide -TiO_2 produced more products as compared to commercial TiO_2, (b) the addition of methanol as a hole scavenger boosted the production of CO but not CH_4, (c) a higher and lower reduction time of IL-RGO as compared to the usual 24 hours of reduction presented basically the same production of CO and CH_4, (d) the positive effect of having an ionic liquid was demonstrated by the double production of CO obtained for IL-RGO-TiO_2 as compared to RGO-TiO_2, and (e) a change in the amount of IL-RGO in the IL-RGO-TiO_2 represented a small difference in the CO production but not in the CH_4

production. This work ultimately demonstrated the huge potential of the utility of a UV-responsive ionic liquid functionalized reduced graphite oxide-TiO_2 nano-composite for the reduction of CO_2 in the presence of H_2O for the production of fuels.

ACKNOWLEDGMENTS

The author would deeply thank Dr. Jean M. Andino for her supervision, advice, patience, and support. The author would also thank the committee members Dr. Erica Forzani and Dr. César Torres for their feedback and valuable time. Likewise, the assistance given by Selisa Rollins and the schematic provided by Phillip Logan are greatly appreciated. Finally, the author wants to dedicate his work to God and his family.

TABLE OF CONTENTS

Page

INTRODUCTION

Energy Consumption and the Increase of Carbon Dioxide Atmospheric Concentration

The United States and the world in general are showing energy and climate problems. Different efforts have been undertaken to decrease energy consumption and to decrease air pollution. It has been reported by the United States Environmental Protection Agency that greenhouse gases principally derive from the burning of fossil fuels in the areas of electricity generation, transportation, and heat[1]. Thus, scientific efforts are targeted towards the use of renewable fuels in order to reduce greenhouse gas emissions.

The U.S. Energy Information Administration predicts that energy consumption will increase by 56 percent by the end of 2040[2]. According to studies, the total world energy consumption will grow from 524 quadrillion British thermal units (Btu) to 820 quadrillion (Btu) by 2040[2]. It is not unreasonable to consider that hydrocarbons will be the primary source of energy for the next decades, but a question remains of whether the current hydrocarbon resources will meet the future demands. The U.S. Energy Information Administration also reports that the energy demand in non-Organization Economic Cooperation and Development (non-OECD) countries will grow by 90% in contrast to active OECD countries where it only will increase by 17% (Figure 1)[2].

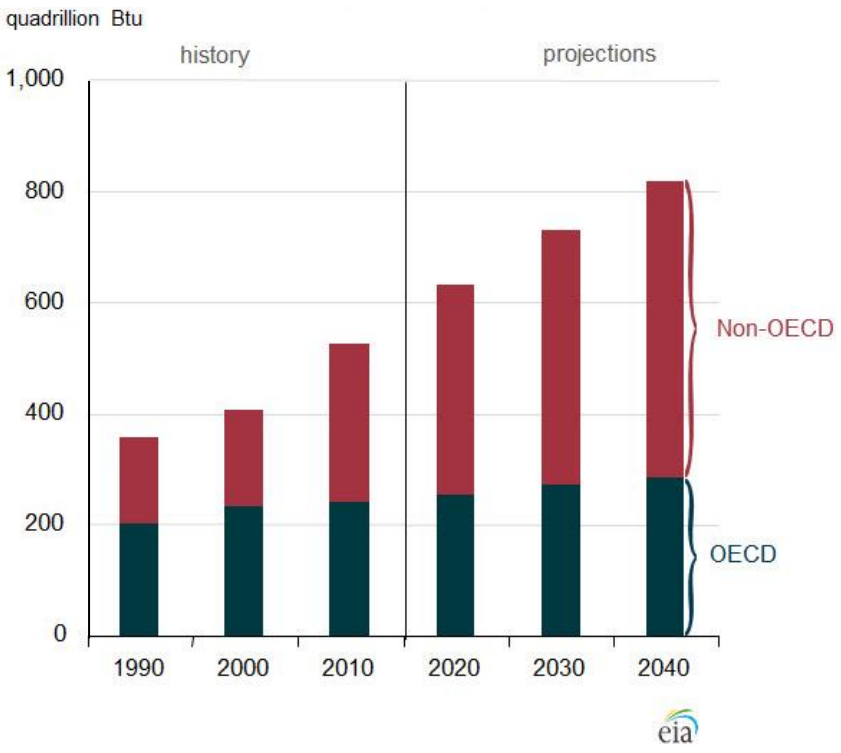

Figure 1. Projected energy consumption until 2040[2]

Renewable energy is projected to be the fastest growing source of energy, with approximately 2.5% growth a year. However, fossil fuels, which currently satisfy 80% of the world's energy demand, are predicted to be a significant source of energy for the next decades[2]. The previous information leads to the suggestion that greenhouse gases such as carbon dioxide (CO_2) will continuously increase in the next years.

The U.S. Energy Information Administration also indicates that in the past 50 to 60 years the United States has consumed more energy as compared to what it is producing. Consequently there is a need to import fuels (for energy generation) from other countries[3]. As illustrated in Figure 2, the gap between the United States' overall production and consumption of energy is prevalent[3].

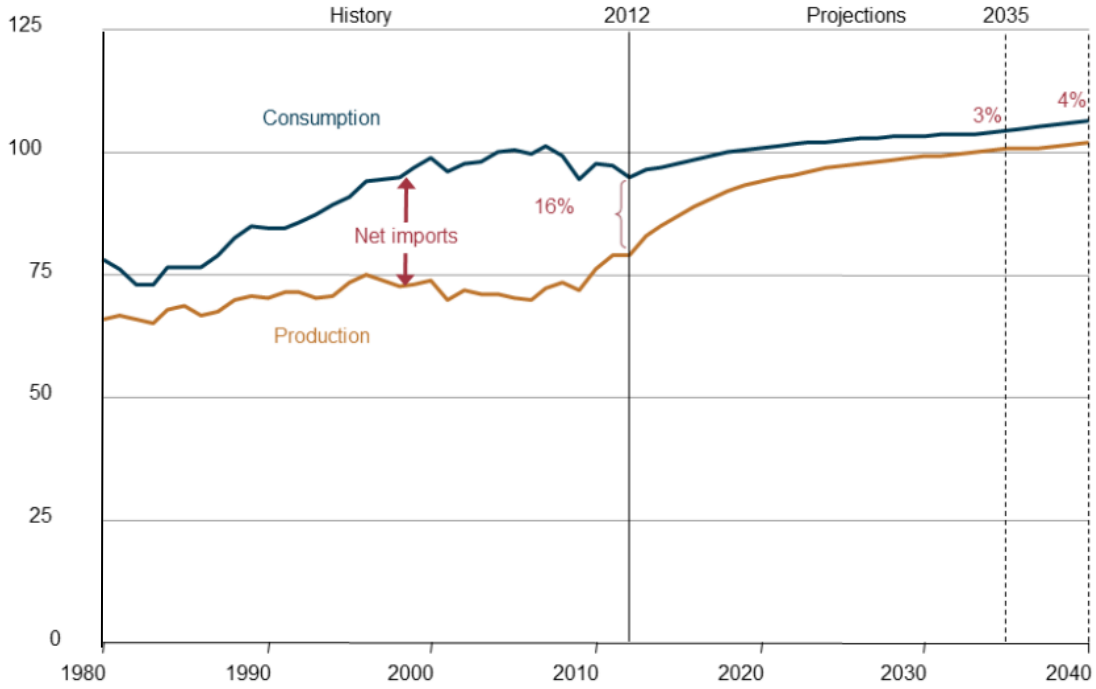

Figure 2. Production and consumption in quadrillion BTU of energy in the U.S.[3]

Among the greenhouse gases emitted in the United States, CO_2 is the major greenhouse gas produced, accounting for 84%[4]. Carbon dioxide is part of the natural Earth carbon cycle, therefore an adequate level of CO_2 is needed. On the other hand, it has been well established by scientific studies that levels of CO_2 higher than normal could lead to global warming problems. The primary sources of CO_2 are from burned fossil fuels, and there has been a dramatic increase in CO_2 production since the 1950's (Figure 3)[5].

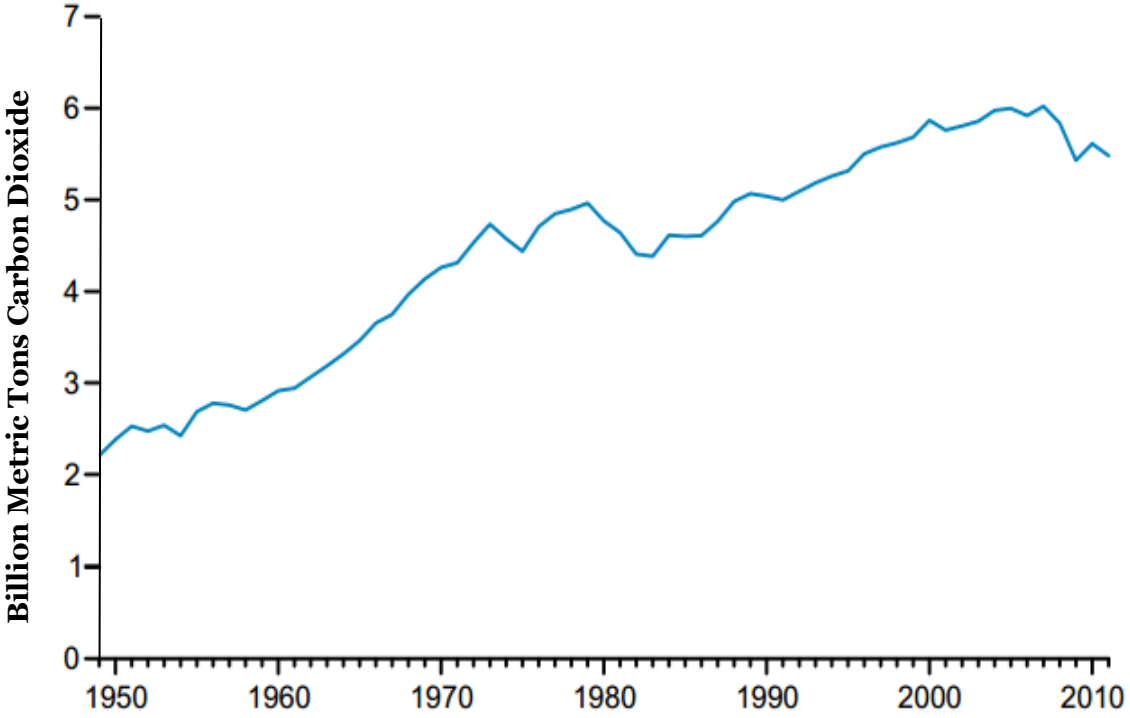

Figure 3. The concentration of CO_2 in the atmosphere increased considerably from 1950 to 2011 due to the use of fossil fuels[5].

The energy needs of humans are affecting the levels of CO_2 in the atmosphere which are leading to environmental problems[4]. Carbon dioxide emissions from fossil fuel usage are influenced by factors such as global climate and economy, technological and population development. In the past 20 years, CO_2 emissions have increased by 10%, which corresponds to the same time period of technology development[1].

Figure 4 displays the sources of CO_2 emissions. Electricity production and hydrocarbons burned for transportation represent about 69% of the CO_2 emissions[1]. Carbon dioxide emissions from industry arise mostly due to the burning of fossil fuels for energy production but also to chemical processes such as cement production.

Commercial and residential CO_2 emissions arise due to fossil fuels that are burned for heat generation. CO_2 emissions in the "Other (non-fossil fuel combustion)" category arise from agricultural sources (e.g. livestock and soil)[1].

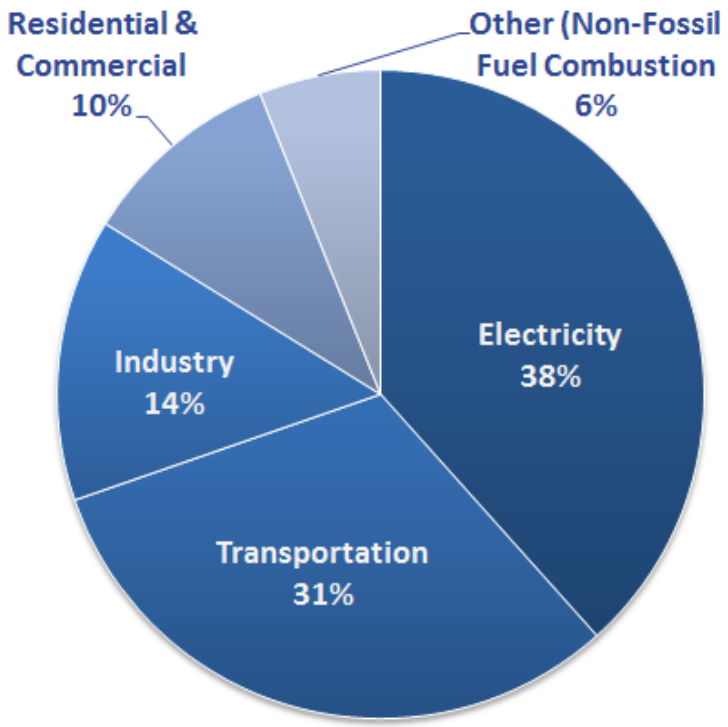

Figure 4. Sources of carbon dioxide emissions in the U.S.[1]

Reduction Strategies for Carbon Dioxide Emissions

The U.S. Environmental Protection Agency (EPA) has suggested different methods to reduce the use of fossil fuels in order to decrease CO_2 emissions. Table 1 describes different strategies to reduce CO_2 emissions, as suggested by the EPA[6].

Table 1. Suggested strategies by the U.S. Environmental Protection Agency (EPA) to reduce carbon dioxide emissions[6]

Strategy	**Examples of how emissions can be reduced**
Energy efficiency	The use of electric or hybrid automobiles, and to have better insolation systems in houses and buildings are ways to increase energy efficiency.
Energy conservation	Turning off all the electronics when not in use, and the use of bicycles.
Fuel switching	The production of renewable fuels such as biofuel and hydrogen is a feasible way to decrease CO_2 emissions.
Carbon capture and sequestration	The capture and sequestration of CO_2 is a technology that can eventually decrease CO_2 emissions.

There is another method to simultaneously deal with the increase in CO_2 emissions, but to also address shortages in global hydrocarbon fuels[7]. The method is the conversion of CO_2 to hydrocarbons or other useful materials. Some of the current technologies that are under investigation for the conversion of CO_2 to fuels are:

hydrogenation and photocatalytic reduction[7-9]. The different hydrocarbon products of CO_2 reduction are presented in reactions 1-4[10].

$$CO_2 + 2H^+ + 2e^- \rightarrow CO + H_2O \quad (1)$$

$$CO_2 + 2H^+ + 2e^- \rightarrow HCO_2H \quad (2)$$

$$CO_2 + 6H^+ + 6e^- \rightarrow CH_3OH + H_2O \quad (3)$$

$$CO_2 + 8H^+ + 8e^- \rightarrow CH_4 + 2H_2O \quad (4)$$

As indicated in reaction 1, carbon monoxide (CO) simply requires two electrons and protons in order to be formed. In consequence, CO production is most common as compared to methane(CH_4)[11]. The production of CO is extremely important since it can be then used to form CH_4 by the process of hydrogenation described in reaction 5[11].

$$CO + 6H^+ + 6e^- \rightarrow CH_4 + 2H_2O \quad (5)$$

Photocatalysis

A photocatalyst is usually a semiconductor that accelerates a light activated reaction[12]. The semiconductors display an energy difference (band gap(E_g)) between the valence band (VB) and a conduction band (CB)[12, 13]. The energy of the band gap is defined as described by equation 1[12].

$$E_c - E_v = E_g \quad \text{(Equation 1)}$$

The activation of a semiconductor is dependent on the absorption of light. The energy needed to activate the photocatalyst has to be the same or higher as compared to

$h\nu$

the band gap energy[13]. Electron (e^-) promotion to the CB and hole (h^+) formation in the VB is achieved by a photon (*hv*) as presented in reaction 6[13].

$$\text{Photocatalyst} \longrightarrow \text{Photocatalyst } (e^- + h^+) \qquad (6)$$

The photoexcitation of an electron in a semiconductor is presented in Figure 5[13].

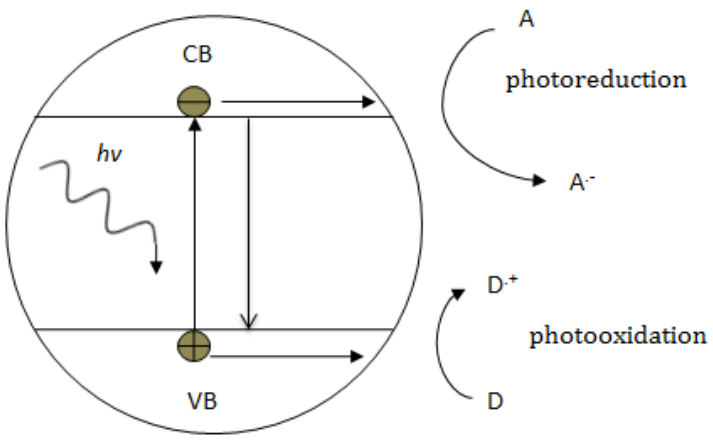

Figure 5. Electron photoexcitation of a semiconductor. Valence band (VB), conduction band (CB), electron accepting species (A), electron donating species (D). Adapted from published studies[13]

The generated electrons and holes can be then utilized for oxidation/reduction reactions[13]. The electrons react with electron acceptor groups, similarly the hole or positive charge in the valence band reacts with electron donor groups[13].

There are several factors that affect the electron/hole production rate. The factors include the following[14]:

1. The intensity of the light used to activate the catalyst
2. The bandgap energy of the semiconductor used
3. The amount of catalyst
4. The temperature and pressure used during the reaction

The proper photocatalyst needs to have the following properties: able to utilize a wide range of light (UV-Visible), economically viable, non-toxic, able to produce enough electrons to reduce CO_2, non-corrosive, and allow for efficient charge separation[14]:

Photocatalytic Reduction of Carbon Dioxide

The most novel, inexpensive and promising method to reduce CO_2 to fuels (C_1-C_2 hydrocarbons) is the use of a photoactivated catalyst in the presence of water vapor (H_2O)[8]. In a typical gas-phase photoreaction, H_2O is oxidized and CO_2 is reduced as reaction 7 illustrates in the photoreduction of CO_2 to CH_4[15].

$$2H_2O + CO_2 \xrightarrow{h\nu} CH_4 + 2O_2 \qquad (7)$$

Ideally, the only energy source that this novel technique would use is solar light in order to be a sustainable approach to effectively deal with CO_2 and enhance fuel production without having a negative effect on the environment[10, 16, 17]. Examples of different semiconductors that can be used as photocatalyst with their respectives bandgap energies are presented in Table 2[14].

Table 2. Photocatalyst compounds and their respective bandgap energies[14, 18]	
Photocatalyst/Bandgap energy (eV)	**Photocatalyst/Bandgap energy (eV)**
Fe_2O_3/3.10	V_2O_5/2.70
α - Fe_2O_3/2.20	Si/1.1
Cds/2.40	TiO_2 (rutile)/3.00
ZnS/3.70	TiO_2 (anatase)/3.20
ZnO/3.20	$SrTiO_3$/3.4
WO_3/2.80	WSe_2/1.2
GaN/3.2	CuO/1.21-1.51
GaAs/1.45	InP/1.34
Cu_2O/2.10	AlP/2.56
TiO_2/3.0-3.3	GaP/2.25

Several publications about CO_2 photoreduction in the presence of H_2O have shown promising results. In a selected group of publications, titania (TiO_2) on zeolites was used as the catalysts where the results demonstrated the formation of CH_4 and methanol (CH_3OH) as primary products and CO as a secondary product [19-21]. The catalysts were irradiated with UV light for several hours and analyzed by gas chromatography[19-21].

Past studies describe the photocatalytic activity of Ti containing thin film porous silica. This work on Ti-thin film porous silica reports the formation of CH_4, CH_3OH and CO[22-24]. The irradiation time was approximately 6 hours using a UV light source with a 100 W Hg lamp and products were analyzed using gas chromatography[22-24].

There is also scientific work that was performed on a variety of catalysts (TiO_2, ZaO, Cds, GaP, SiC and WO_3O) for the photoelectrocatalytic reduction of CO[25]. The work was performed using the semiconductors suspended in H_2O[25]. The light sources were a 500 W Xe lamp and a 500 W high pressure mercury arc lamp. The main products were formaldehyde and CH_3OH. Secondary products were formic acid, CH_4 and methyl alcohol[25]. The product yields were ~$5.0x10^{-4}$ M for HCHO and $1.9x10^{-4}$ M for CH_3OH using a TiO_2 catalyst, and $5.0x10^{-4}$ M for HCHO and $4.5\ x10^{-4}$ M for CH_3OH using a SiC catalyst[25].

Up to now, the most studied photocatalytic material for CO_2 conversion has been titanium dioxide (TiO_2) because it has provided the highest efficient photocatalytic activity, and has other various advantages such as being thermally stable, economically feasible and non-toxic[26, 27].

Photocatalytic Properties of TiO_2

There are several properties that make titanium dioxide (TiO_2) a useful photocatalytic material[28]. One of the most important characteristics of TiO_2 is the availability of the material since TiO_2 ranks as the fourth most plentiful material on Earth[29].

Studies on the photocatalytic properties of TiO_2 started as early as the 1950s, but it was not until the 1970s when Fujishima and Honda discovered the ability to achieve H_2O splitting on TiO_2[30]. Since then, efforts have been made to understand the photocatalytic mechanism and to improve the photocatalytic activity of TiO_2.

Titanium dioxide is usually synthesized in three principal crystallographic structures: rutile (tetragonal), anatase (tetragonal) and brookite (orthorhombic) as described in Figure 6[30, 31]. However, the two crystal phases of TiO_2 that are generally used as photocatalyst are anatase and rutile. Geometric defects have shown to directly disturb the conductive properties of the TiO_2 surface[30].

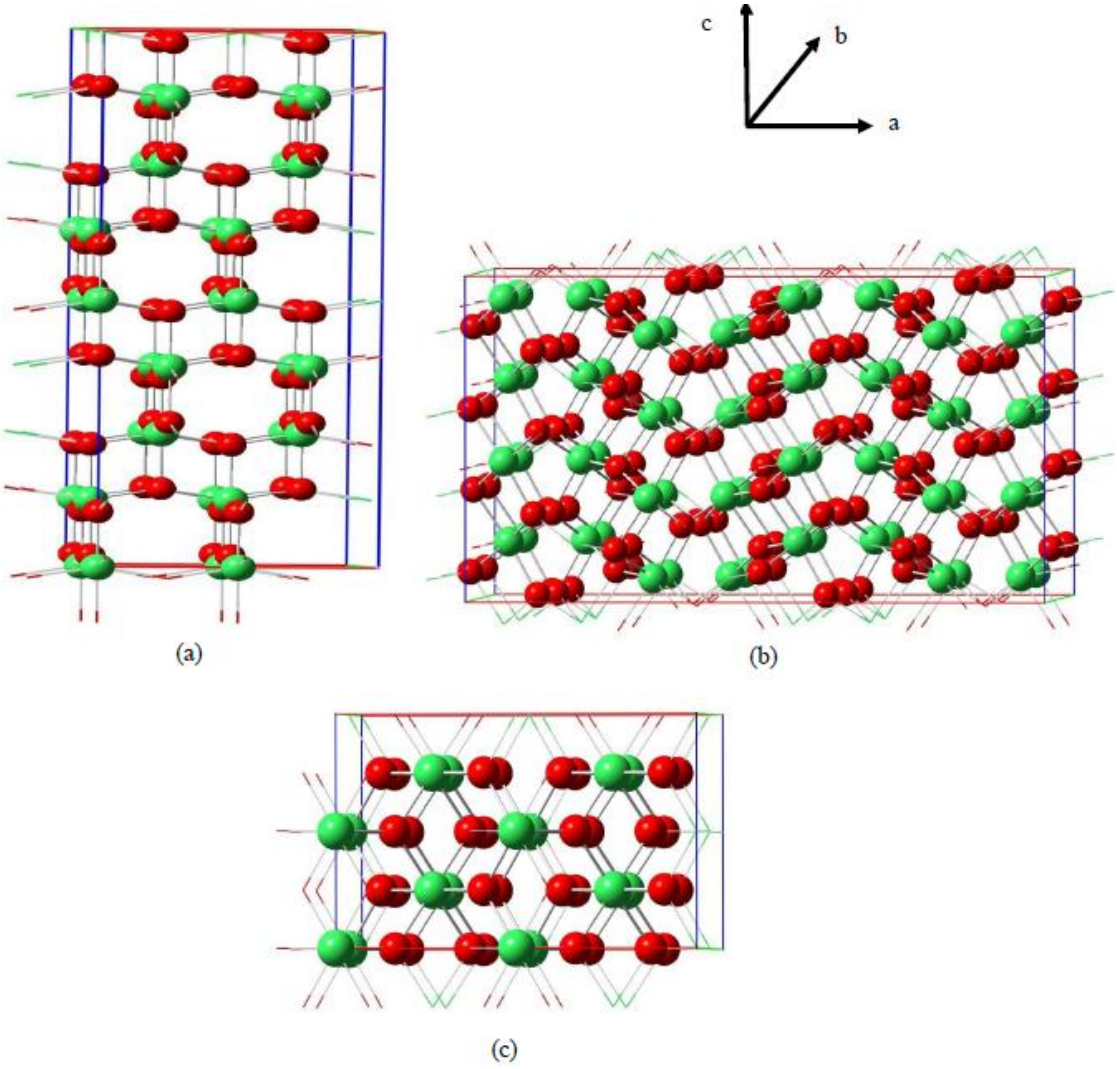

Figure 6. Principal TiO_2 crystallographic structures: (a) anatase, (b) brookite and (c) rutile. Ti atoms are in red and O atoms are in green.

The capacity to regulate surface defects such as oxygen vacancies by heat treatment and photon bombardment in order to introduce charges on the TiO_2 surface is one of the primary photocatalytic features of TiO_2[30, 32]. The most used commercial form of TiO_2 (e. g. Evonik P25) is a combination of approximately 75 percent anatase and 25 percent rutile. The 72%:25% anatase:rutile mixture of TiO_2 has shown promising results for CO_2 photoreduction[33-36].

There are different problems that affect the photocatalytic activity of TiO_2. One issue being that the bandgap energy of TiO_2 (~3.2eV) corresponds to the energy of UV light, consequently TiO_2 can only be activated by UV light. Given that UV light is less than 5% of the electromagnetic spectrum, the use of TiO_2 for CO_2 photocatalytic reduction is not very efficient[30]. Another problem that TiO_2 faces is the low efficiency of the photocatalytic reaction as a result of the rapid recombination between the photogenerated holes and electrons[28].

In order to overcome the fast electron/hole recombination, TiO_2 is usually modified with various materials. Modification of the TiO_2 helps to capture the excited electron on an “electron trapper”, with the purpose of promoting charge separation (Figure 7)[36]. In addition, modifying TiO_2 might cause reduction of the bandgap energy leading to the expansion of the usable frequencies for activation to the visible light range[37].

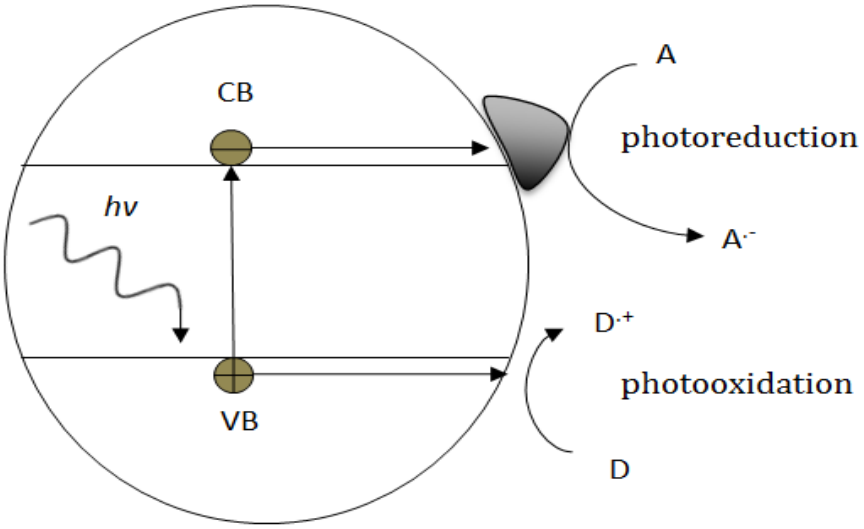

Figure 7. The effect of a modified (dark gray circle) -TiO_2 on the excited electron. Adapted from published studies[36].

Some of the TiO_2 modifiers include: the deposition of transition metals, such as copper, iron, iodine, silver, gold, platinum or their oxides into the photocatalysts structure[28]. Modifying TiO_2 with metals has revealed a dramatic improvement in its photocatalytic activity[38].

The properties that constitute a proper TiO_2 modifier include[39, 40]:

1. High conductivity in order to be able to "trap" the electron
2. High surface area
3. Low cost
4. Non-toxicity
5. Availability

Carbon Nano-Materials as TiO_2 Modifiers

New work on modified TiO_2 has demonstrated an enhancement of TiO_2 photocatalytic activity when incorporating carbon nano-materials to TiO_2[38]. Carbon nanotubes (CNTs) and graphene (sp^2 carbon layer) are the principal carbonaceous nano-materials that have been studied due to their conductivity, surface area and molecular stability[41]. The enhancement of TiO_2 photocatalytic activity using the carbon nano-materials is credited to the adsorption of UV-Vis light and electron trapping[41].

Graphene exhibits smaller electron transfer obstruction as compared to CNTs, thus minimizing electron/hole recombination[42]. Graphene is a single hexagonal carbon layer that has a sp^2 structure (Figure 8, top left) and extraordinary properties such as a large theoretical surface area (2630 m^2/g), high Young's Modulu's and high conductivity[43].

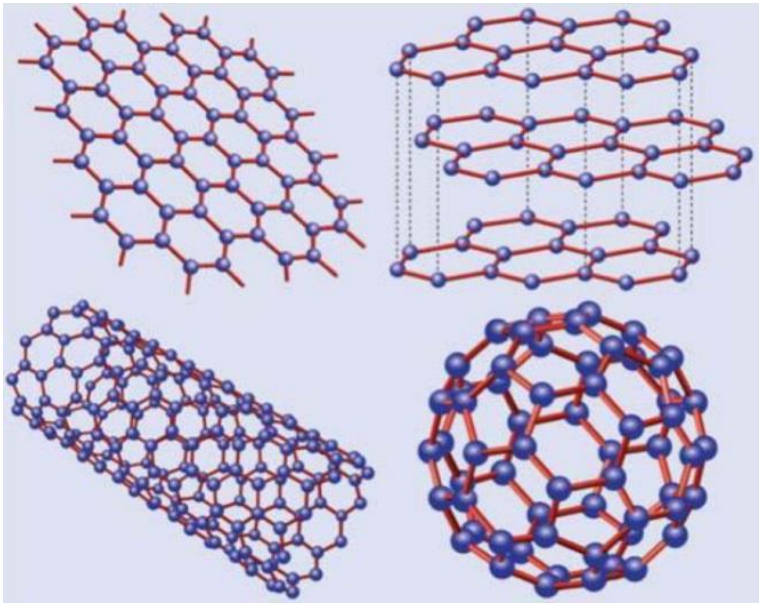

Figure 8. Structures of graphene (top left), graphite (top right), carbon nano -tubes CNTs (bottom left) and fullerenes (bottom right)[44, 45]

One method used to synthesize graphene layers is by reducing graphite oxide[46]. Graphite oxide has a sp^3 structure with different oxygen-containing groups such as epoxide and hydroxyl that provide hydrophilic properties to the graphene oxide[43]. A large improvement in photocatalytic activity has been reported when using reduced graphite oxide (RGO), since this material serves as an electron trapper in a reduced graphite oxide modified TiO_2 nano-composite[47]. There are very few publications regarding the use of UV-vis light activated nanocarbon modified TiO_2 catalysts for the conversion of CO_2 and H_2O to fuels, however their fuel production is minimum (Table 3).

Table 3. Publications of carbon dioxide photocatalytic reduction to hydrocarbons using nanocarbon-TiO_2 catalysts

Catalyst	Type of light	Amount of catalyst	Type of reactor	Time of pre treatment	Temperature of pretreatment	Products $\mu mol g_{catalyst}^{-1} h^{-1}$	Reference
TiO_2/ graphene	UV light, 300W Xenon lamp	0.1 g	Batch	2 hours under nitrogen	300°C	Methane 10.1 Ethane 16.8	[48]
Hollow spheres: titania nanosheets and graphene	300 W xenon arc lamp	0.01 g	Batch	1 hour at vacuum	350°C	CO 8.91 Methane 1.14	[49]
Carbon-titania nanosheet	UV-Visible	N/R*	Batch	30 min in air	400°C	Methane 9.0	[50]
Graphene-TiO_2	UV and visible	Different weight percent	Batch	30 min in air	400°C	Methane 8.5	[41]
Carbon nanotubes on Ni-TiO_2	Visible light	N/R*	Batch	2 hour under methane and H_2/Ar	750°C	Methane 0.145	[51]
Milti-walled carbon nanotube supported TiO_2	UV	N/R*	Batch	2 hours under argon	450°C	Methane 73.33 Formic acid 93.35 Ethanol 149.36	[52]

*No amount reported

Research Objectives

The work outlined in this document focuses on understanding the reactivity of CO_2 over a new UV light activated carbon-TiO_2 nanocomposite in the presence of H_2O. It was hypothesized that modifying TiO_2 with a highly conductive surface like an ionic liquid functionalized reduced graphite oxide (IL-RGO) would not only minimize charge recombination but also selectively attract CO_2 in order to enhance product formation. This catalyst is the first to use an ionic liquid functionalized reduced graphite oxide as a TiO_2 modifier for CO_2 conversion to fuels in the presence of H_2O. To test the hypothesis the following activities were performed:

1. To demonstrate that the IL-RGO-TiO_2 composite would lead to higher product production as compared to unmodified TiO_2 or a reduced graphite oxide (RGO)-TiO_2 material, a gas chromatograph (GC) with a flame ionization detector (FID) and a thermal conductivity detector (TCD) was used.
2. Experiments using the GC were conducted to determine if IL-RGO-TiO_2 surfaces containing the IL-RGO reduced for different periods of time or containing different IL-RGO weight percentages enhanced CO_2 photocatalytic reduction to valuable products.
3. Also, experiments were performed to determine if the addition of a commonly used hole scavenger such as methanol would enhance the photocatalytic activity of the new catalyst.

The eventual objective of this work was to demonstrate that an ionic liquid functionalized reduced graphite oxide-titanium dioxide would be an effective catalyst for the photocatalytic conversion of CO_2 to fuels.

METHODS

Catalyst Synthesis

The catalytic material was synthesized in-house using methods modified from Kovtyukhava, *et al.*[53], Hummers and Offeman[54], and Yang, *et al.*[55]. Carbon layers were separated by oxidizing graphite. Prior to oxidizing graphite, a pre-oxidation was needed in order to obtain a higher yield of graphite oxygenated nano-particles, similar to work performed by Kovtyukhava, *et al.*[53]. Pre-oxidation of graphite was obtained by adding graphite powder to a mixture of H_2SO_4, $K_2S_2O_8$ and P_2O_5 at 80°C. A dark solution was obtained. The dark solution was allowed to cool down to room temperature for six hours in a standalone stirrer. Then the solution was washed with nanopure water until the pH became neutral. Finally, the pre-oxidized graphite was dried at 35°C overnight.

Graphite oxide (GO) was obtained by using a method from Hummers and Offeman[54]. The dried pre-oxidized graphite oxide was added to a mixture of H_2SO_4 and $KMnO_4$ at 0°C and stirred for 10 minutes. After that, the mixture was then stirred at 35°C for two hours. After the two hours, nanopure water was added to the mixture, and was allowed to stir for 15 minutes. Next, nanopure water and 30% H_2O_2 were added to the oxidized graphite, resulting in a bright yellow color (see appendix). The bright yellow solution was washed with HCl and H_2O (1:10 HCl to H_2O volume ratio). The dark brown viscous product was suspended in nanopure water. The suspended GO was washed with nanopure water to eliminate the excess HCl. Finally, nanopure water was added to the resultant neutral GO. Graphite oxide is non-conductive[56]. Thus, in order to gain conductivity, graphite oxide must be reduced[56].

Ionic liquids have a strong ability to attract CO_2 and are highly soluble in H_2O[57]. These two properties make them a powerful tool for CO_2 photocatalytic reduction to

fuels. In the catalyst used in the present document, at the same time that reduction of graphite oxide occurred, graphite oxide was functionalized with a NH_2 terminated ionic liquid 1-butyl-3-methylimidazolium chloride (NH_2-C_4mimCl). The high solubility of the ionic liquid in H_2O and its charge repulsion makes it a viable way for TiO_2 to be dispersed and decorated on the ionic liquid functionalized reduced graphite oxide (IL-RGO) sheets[55]. The theoretical surface area of the IL-RGO may enhance the adsorption of the photocatalytic reactants, subsequently generating more reactive sites. Previous work conducted by Andino's research group points out that the NH_2-C_4mimCl ionic liquid does not interact with alkanes[58]. For that reason, the ionic liquid might selectively attract CO_2 to interact with the excited electrons, and rapidly dissociate any potential hydrocarbon products.

The ionic liquid (IL) was synthesized by containing a mixture of 3-chloropropylamine hydrochloride, 1-methylimidazole and ethanol refluxing under nitrogen and stirrer for 24 hours at ~80^{O}C (see appendix). Then, ethyl acetate was added to the mixture resulting in a cloudy turbid mixture (see appendix) which was dried under nitrogen at ~60^{O}C for 24 hours[55]. An image of the resulting ionic liquid (NH_2 terminated 1-butyl-3-methylimidazolium chloride (NH_2-C_4mimCl)) is shown in the appendix.

IL-reduced graphite oxide (RGO) synthesis was accomplished using a modified method from Yang, *et al.*[55]. To obtain the IL-RGO, GO was added to the ionic liquid resulting in a brown turbid mixture (see appendix). In order to allow the epoxide ring opening to occur, KOH was added to the IL-GO mixture and then it was ultrasonicated for 1 hour. During the ultra-sonication the mixture started to change to a dark brown color due to an increase in temperature (see appendix). The color change suggested that graphite oxide reduction was successfully starting to happen. The dark brown solution

was stirred for 24 hours at 80^{0}C under nitrogen to have complete reduction of the oxidized graphite (see appendix). The resulting dark turbid mixture was washed with 1:10 ethanol to H_2O volume ratio.

Lastly, a mixture of C_4mimBF_4 and H_2O was added to TiO_2 in order to enhance the dispersion of the TiO_2 nanoparticles[59]. The product was allowed to stir for one hour. The washed IL-RGO was ultrasonicated for 30 minutes. Right after the ultra-sonication, the IL-RGO was added to the $TiO_2/C_4mimBF_4/H_2O$ mixture and stirred for one more hour. Then the mixture was washed with a 1:10 ethanol to H_2O mixture. The final product, which was the IL-RGO-TiO_2, was dried at 80°C for 24 hours to remove ethanol from the surface (see appendix for image of the IL-RGO-TiO_2).

The RGO-TiO_2 catalyst was synthesized using the same procedure as the IL-RGO-TiO_2, but neither of the two ionic liquids (used for the IL-RGO-TiO_2) were added.

Chemicals Used

Graphite flake (325 mesh, 99.8%), potassium permanganate and methanol (99.8+%) were purchased from Alfa Aesar. 3-Chloropropylamine hydrochloride (98%), 1-methylimidazole (≥99%), 1-butyl-3-methylimidazolium tetrafluoroborate (C4mimBF4, ≥98%), phosphorous pentoxide (98%), potassium hydroxide (85%), P-25 (titanium (IV) oxide 99.5%), ethyl acetate (99.8%, anhydrous) and ethanol (≥99.5%) were purchased from Sigma Aldrich. Hydrogen peroxide (30%) was purchased from Fisher Scientific. Sulfuric acid (98%) and hydrochloric acid (38%) were purchased from EMD Millipore.

Characterization

Brunauer–Emmett–Teller (BET)

The modification of the TiO_2 with the IL-RGO should increase the surface area of the catalyst. A higher surface area represents more reactive sites for CO_2 conversion. A Micromeritics' TriStar II was used to determine the BET surface area of the catalysts. The instrument operated using the nitrogen gas adsorption method.

Raman spectroscopy

A Raman spectrometer having 180° geometry specially built at Arizona State University was used to study the molecular vibrational modes of the catalysts. Raman spectroscopy gave information on the oxidation of graphite and reduction of graphite oxide by looking at the sp^2 and sp^3 carbon structures. The Raman spectrometer utilized a 100mW Compass 532 nm laser controlled by neutral density filters to excite the sample. A 50X super long working distance Mitutoyo objective with a numerical aperture of 0.42 was used to focus the laser. The signal was filtered using a Kaiser Laser band pass filter and a Semrock edge filter. Data were collected by an Acton 300i spectrograph and a back-thinned Princeton Instruments liquid N_2 cooled CCD detector.

UV-visible (UV-vis) absorption spectroscopy

UV-vis absorption spectra were obtained using a UV–visible spectrophotometer (Perkin-Elmer LAMBDA-18). The spectra were used to determine the effect that coupling TiO_2 with IL-RGO had on the composite's bandgap energy.

X-ray photoelectron spectroscopy (XPS)

The XPS data were acquired to characterize the surface atomic concentration. The XPS data also helped to demonstrate the reduction of graphite oxide. The study was performed with a VG ESCALAB 220i-XL aluminum-K α (1486.6 eV) X-ray source.

Photocatalytic Experiments

The photocatalytic experiments were performed in a 100mL quartz glass batch reactor. The reactor was placed inside a Srinivasan-Griffin Rayonet photochemical reactor to have a uniform UV irradiation and the proper ventilation. Water vapor was produced by flowing nitrogen/helium through an impinger containing nanopure water. Figure 9 illustrates the reactor setup for the photocatalytic experiments.

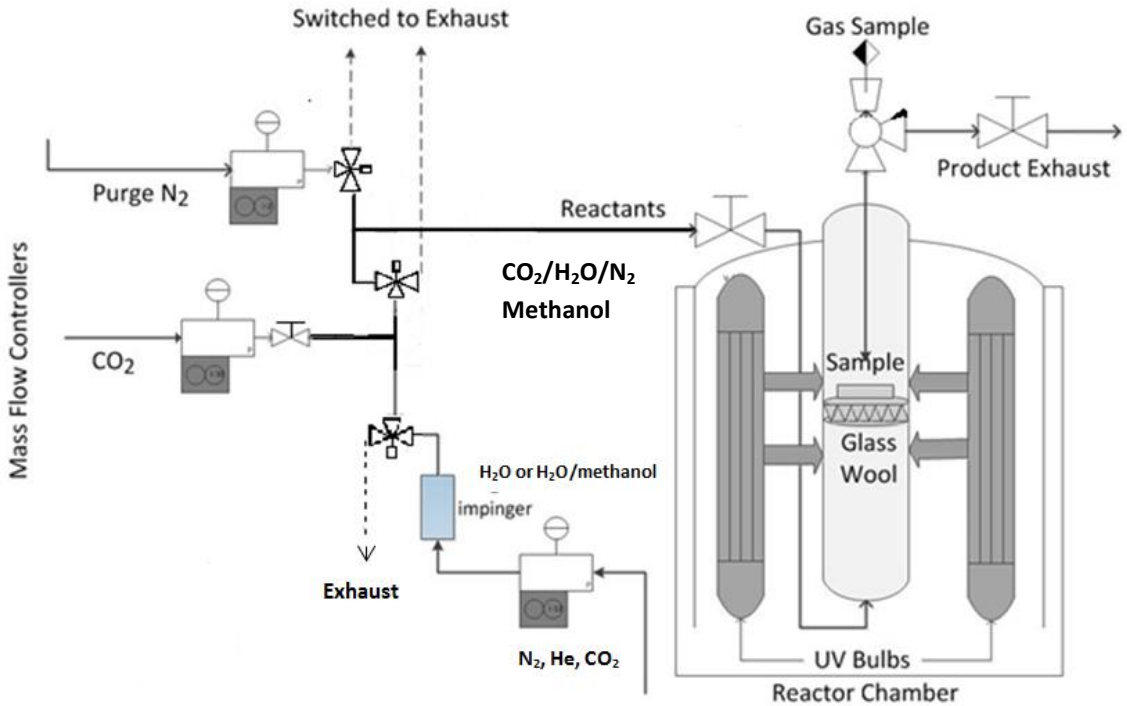

(Srinivasan-Griffin Rayonet)

Figure 9. Reactor setup

A gas chromatograph mounted with a TCD and FID is the preferable technique to study the products from the photocatalytic experiments, as presented in Table 4.

Table 4. Techniques used to investigate the performance of CO_2 photoreduction to fuels

Method	Catalysts	Results	Reference
Gas chromatography-FID	TiO_2/RuO_2	HCOOH(1.46μmol/hr), CH_3OH(0.21 μmol/hr), HCHO(0.17 μmol/hr)	[60]
Gas chromatography-FID (Yanako G2800 and GL Science GC-380)	TiO_2/Cu	CH_4(15μl/g), C_2H_6(22μl/g)	[61]
Gas chromatography, mass spectrometry, high pressure liquid chromatography	TiO_2/RuO_2/Ru	CH_4(450μl)	[62]
HP 5890 gas chromatography-FID-TCD, Ion chromatography	TiO_2/Pd	H_2 (5.2×10^{-2} μmol/min)	[63]

A Bruker 456 gas chromatography (GC) mounted with a thermal conductivity detector (TCD) and a flame ionization detector (FID) was used to determine and quantify the photocatalytic products. The GC section of the instrument is used to separate components of the mixture. After separation, each component enters the detector region. The thermal conductivity detector measures the difference in thermal conductivities of the carrier gas flow and the sample gas flow[64]. Any compound that has a thermal conductivity that is different from the thermal conductivity of the carrier gas may be measured with a TCD detector[64]. A compound that enters the flame ionization detector (FID) passes through a hydrogen flame where it is burned, thus producing ions[65]. The ions create an electrical signal which is then measured[65].

The GC that was used in this work is fixed with two columns: a fused silica Q-plot column and a mol-sieve column. The Q-plot column has dimensions of 30m x 0.53mm (length x internal diameter) and an average film thickness of 20μm to separate C1 to C3 isomers and alkanes up to C12. The maximum operating temperature is 300°C. The mol-sieve column has dimensions of 15m x 0.53mm (length x internal diameter) and an average film thickness of 50μm to separate oxygen, nitrogen, carbon monoxide and methane. The maximum operating temperature is 300°C.

The experiments that were carried out to compare commercial TiO_2 versus IL-RGO-TiO_2 at different pretreated conditions are described in Table 5.

Table 5. Methodology of the experiments performed to analyze the photocatalytic performance of IL-RGO-TiO_2 versus commercial TiO_2

IL-RGO-TiO_2 untreated	**IL-RGO-TiO_2 pretreated 120°C**	**IL-RGO-TiO_2 pretreated 200°C**	**TiO_2 pretreated 200°C**	**TiO_2 untreated**
• 0.5560g of IL-RGO-TiO_2 • Room temperature (21°C) • N_2 purge 140 min • N_2 + H_2O + CO_2 purge 30 min • N_2 + H_2O + CO_2 (~7%v/v CO_2 and ~2%v/v H_2O) batch 15 min no light • UV light • Quartz reactor (100ml)	• 0.4875g of IL-RGO-TiO_2 • IL-RGO-TiO_2 pretreated at 120°C under nitrogen for 90 minutes • Allowed to cool down to room temperature (21°C) • Total N_2 purge 150 min • N_2 + H_2O + CO_2 purge 30 min • N_2 + H_2O + CO_2 (~7%v/v CO_2 and ~2%v/v H_2O) batch 15 min no light • UV light • Quartz reactor (100ml)	• 0.5360g of IL-RGO-TiO_2 • IL-RGO-TiO_2 pretreated at 200°C under nitrogen for 90 minutes • Allowed to cool down to room temperature (21°C) • Total N_2 purge 130 min • N_2 + H_2O + CO_2 purge 30 min • N_2 + H_2O + CO_2 (~7%v/v CO_2 and ~2%v/v H_2O) batch 15 min no light • UV light • Quartz reactor (100ml)	• 0.4946g of TiO_2 • TiO_2 pretreated at 200°C under nitrogen for 90 minutes • Allowed to cool down to room temperature (21°C) • Total N_2 purge 130 min • N_2 + H_2O + CO_2 purge 30 min • N_2 + H_2O + CO_2 (~7%v/v CO_2 and ~2%v/v H_2O) batch 15 min no light • UV light • Quartz reactor (100ml)	• 0.4997g of TiO_2 • Room temperature (21°C) • N_2 purge 130 min • N_2 + H_2O + CO_2 purge 30 min • N_2 + H_2O + CO_2 (~7%v/v CO_2 and ~2%v/v H_2O) batch 15 min no light • UV light • Quartz reactor (100ml)

The experiments to determine if adding methanol enhanced the photocatalytic activity of the IL-RGO-TiO_2 (towards CO_2 conversion) are described in Table 6.

Table 6. Methodology of the experiments performed to analyze if adding a hole scavenger such as methanol will improve the photocatalytic performance of IL-RGO-TiO_2

(0.5g) TiO_2 and IL-RGO-TiO_2 (0.84% v/v methanol)	**(0.5g) TiO_2 (0.84% v/v methanol) (No CO_2)**	**(0.5g) TiO_2 and IL-RGO-TiO_2 (0.61% v/v methanol)**	**(0.2g) TiO_2 and IL-RGO-TiO_2 (0.61% v/v methanol)**
• 0.4915g for TiO_2 and 0.4947g for IL-RGO-TiO_2 respectively • Pretreated (200^{O}C) under helium for 2 hr. • Allowed to cool down to room temperature for 1 hr. • (99%) CO_2 flow through a H_2O (140mL)/methanol (10mL) bath for 5 min before batch mode (100mL/min) • methanol + H_2O + CO_2 batch 10 min no light (2.2%v/v H_2O and 96.2%v/v CO_2) • UV light (450 W) • Quartz reactor (100ml)	• 0.4891g of TiO_2 • Pretreated (200^{O}C) under helium for 2 hr. • Allowed to cool down to room temperature for 1 hr. • (99.99%)He flow through a H_2O (140mL)/methanol (10mL) bath for 5 min before batch mode (100mL/min) • methanol + H_2O + Helium batch 10 min no light (2%v/v H_2O and 97%v/v He) • UV light (450 W) • Quartz reactor (100ml)	• 0.5003g for TiO_2 and 0.4959 for IL-RGO-TiO_2 respectively • Pretreated (200^{O}C) under helium for 2 hr. • Allowed to cool down to room temperature for 1 hr. • (99%) CO_2 flow through a H_2O (95mL)/methanol (5mL) bath for 1 hour before batch mode (4mL/min) • methanol + H_2O + CO_2 batch 5 min no light (2.2%v/v H_2O and 96.2%v/v CO_2) • UV light (450 W) • Quartz reactor (100ml)	• 0.1997g for TiO_2 and 0.2011 for IL-RGO-TiO_2 respectively • Pretreated (200^{O}C) under helium for 2 hr. • Allowed to cool down to room temperature for 1 hr. • (99%) CO_2 flow through a H_2O (95mL)/methanol (5mL) bath for 1 hour before batch mode (4mL/min) • methanol + H_2O + CO_2 batch 5 min no light (2.2%v/v H_2O and 96.2%v/v CO_2) • UV light (150 W) • Quartz reactor (100ml)

The experiments performed to determine if a higher or lower reduction time as compared to the usual 24 hours used for the reduction of the IL-RGO would enhance the photocatalytic properties of the IL-RGO-TiO_2 are described in Table 7.

Table 7. Methodology of the experiments performed to analyze how different time periods for the reduction of IL-RGO will impact the photocatalytic performance of IL-RGO-TiO_2

IL-RGO-TiO_2 IL-RGO (12 hours reduction)	**IL-RGO-TiO_2 IL-RGO (24 hours reduction)**	**IL-RGO-TiO_2 IL-RGO (48 hours reduction)**	**IL-RGO-TiO_2 IL-RGO (62 hours reduction)**
• 0.1120g of IL-RGO-TiO_2 • Room temperature (21^oC) • N_2 purge 60 min • $N_2 + H_2O + CO_2$ purge 15 min • $N_2 + H_2O + CO_2$ (~1%v/v CO_2 and ~2%v/v H_2O) batch 5 min no light • UV light • Quartz reactor (100ml)	• 0.1013g of IL-RGO-TiO_2 • Room temperature (21^oC) • N_2 purge 60 min • $N_2 + H_2O + CO_2$ purge 15 min • $N_2 + H_2O + CO_2$ (~1%v/v CO_2 and ~2%v/v H_2O) batch 5 min no light • UV light Quartz reactor (100ml)	• 0.1113g of IL-RGO-TiO_2 • Room temperature (21^oC) • N_2 purge 60 min • $N_2 + H_2O + CO_2$ purge 15 min • $N_2 + H_2O + CO_2$ (~1%v/v CO_2 and ~2%v/v H_2O) batch 5 min no light • UV light Quartz reactor (100ml)	• 0.1120g of IL-RGO-TiO_2 • Room temperature (21^oC) • N_2 purge 60 min • $N_2 + H_2O + CO_2$ purge 15 min • $N_2 + H_2O + CO_2$ (~1%v/v CO_2 and ~2%v/v H_2O) batch 5 min no light • UV light Quartz reactor (100ml)

The experiments performed to analyze the photocatalytic effect of the ionic liquid in the IL-RGO-TiO_2 for the conversion of CO_2 to fuels are described in Table 8.

Table 8. Methodology of the experiments performed to analyze how the ionic liquid will impact the photocatalytic performance of IL-RGO-TiO_2

IL-RGO-TiO_2	**RGO-TiO_2**
• 0.1013g of IL-RGO-TiO_2 • Room temperature (21^{O}C) • N_2 purge 60 min • N_2 + H_2O + CO_2 purge 15 min • N_2 + H_2O + CO_2 (~1%v/v CO_2 and ~2%v/v H_2O) batch 5 min no light • UV light • Quartz reactor (100ml)	• 0.1080g of RGO-TiO_2 • Room temperature (21^{O}C) • N_2 purge 60 min • N_2 + H_2O + CO_2 purge 15 min • N_2 + H_2O + CO_2 (~1%v/v CO_2 and ~2%v/v H_2O) batch 5 min no light • UV light • Quartz reactor (100ml)

The experiments performed to analyze how using different IL-RGO weight percentages in the IL-RGO-TiO_2 composite would impact the photocatalytic production of products are described in Table 9.

Table 9. Methodology of the experiments performed to analyze how different weight percentages of IL-RGO affect the photocatalytic performance of IL-RGO-TiO_2

IL-RGO(0.3 wt.%)-TiO_2	**IL-RGO(0.2 wt.%)-TiO_2**	**IL-RGO(0.1 wt.%)-TiO_2**
• 0.1054g of IL-RGO-TiO_2 • Room temperature (21^0C) • He purge 60 min • N_2 + H_2O + CO_2 purge 15 min • N_2 + H_2O + CO_2 (~1%v/v CO_2 and ~2%v/v H_2O) batch 5 min no light • UV light • Quartz reactor (100ml)	• 0.1113g of IL-RGO-TiO_2 • Room temperature (21^0C) • He purge 60 min • N_2 + H_2O + CO_2 purge 15 min • N_2 + H_2O + CO_2 (~1%v/v CO_2 and ~2%v/v H_2O) batch 5 min no light • UV light • Quartz reactor (100ml)	• 0.1119g of IL-RGO-TiO_2 • Room temperature (21^0C) • He purge 60 min • N_2 + H_2O + CO_2 purge 15 min • N_2 + H_2O + CO_2 (~1%v/v CO_2 and ~2%v/v H_2O) batch 5 min no light • UV light Quartz reactor (100ml)

RESULTS AND DISCUSSION

Characterization Results

Raman spectroscopy was performed to characterize the graphite oxide and the IL-RGO-TiO_2 and results were plotted in Figure 10. The results show the existence of the "D" band and the "G" band. The G band corresponds to the sp^2 bonded carbon atoms and the D band corresponds to disordered sp^3 bonded carbon atoms[46]. The Raman spectra reveal shifts at~1354 cm^{-1} and 1581 cm^{-1} for the D and G bands of the graphite oxide. After the reduction of graphite oxide, the peaks moved to lower values of ~1345 cm^{-1} and 1578 cm^{-1} for the D and G bands. According to literature, the broadening of the G and D peaks suggest an oxidation of graphite[46]. The relative intensity D/G band ratio is 1.032 for GO and the relative intensity D/G band ratio is 0.96 for IL-RGO-TiO_2. The D/G band intensity ratio decrease is indicative of the rebuilding of some sp^2 carbon structures[48, 66]. The rebuilding of sp^2 carbon structures suggests a gain in conductivity[67]. The virtually small D/G band intensity ratio decrease could be attributed to the attachment of the ionic liquid on the carbon layers, since the attachment of the ionic liquid might increase the D band intensity[46].

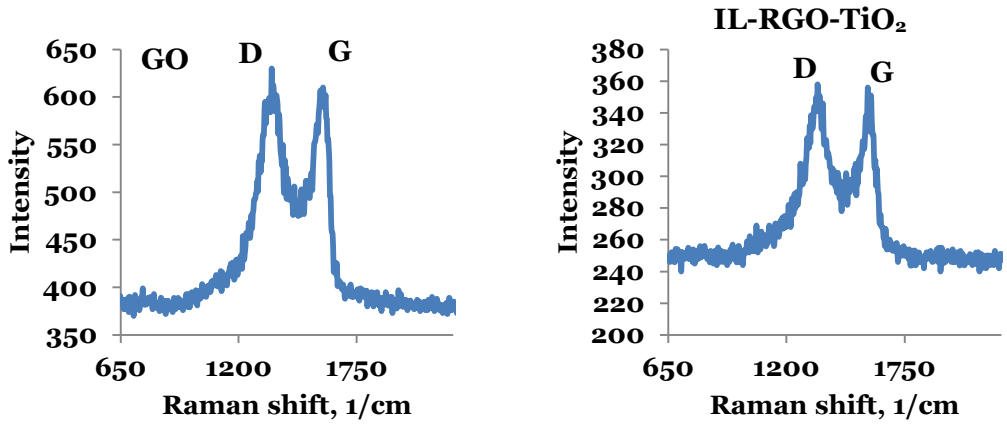

Figure 10. Raman spectroscopy spectra for GO (left) and IL-RGO (right)

X-ray photoelectron spectroscopy (XPS) characterization was performed to determine the chemical composition of GO, IL-RGO, and IL-RGO-TiO_2. The wide scan survey of graphite oxide (GO), IL-RGO, and IL-RGO-TiO_2 (Figures 11, 12, and 13) showed that the anticipated elements O and C for graphite oxide, O, C, and N for IL-RGO and O, C, N, and Ti for IL-RGO-TiO_2 were present in the catalysts.

The carbon peak is comprised of different binding configuration C=C, C-C, C=O, C-OH, and epoxide/ether, as displayed in Figures 14 and 15. Figures 14 and 15 also demonstrate the reduction of the epoxide/ether bonds, which occurred when GO was reacted with KOH and NH_2-C_4mimCl in the presence of heat. An accompanying increase in the signals corresponding to C=C and C-C configurations (reduction of graphite oxide) occurred. In addition, Table 10 validates that the C/O ratio increased from 3.00 to 6.35 in the chemical process of converting from GO to IL-RGO. Thus, many oxygen groups on the GO disappeared; supporting the information that GO was reduced. Table 10 illustrates the expected result that the C/O ratio increased as the reduction time of IL-RGO increased due to the higher exposure time to heat[68]. The difference in weight percent of IL-RGO also shows a difference in the atomic percent of carbon (Table 10).

The evidence of the N1s band at ~400 eV with a lower binding-energy shoulder at ~398 eV in the high resolution spectrum of IL-RGO and IL-RGO-TiO_2 (Figures 16 and 17) is in accordance with literature[55]. The N1s band, together with the C-N peak at 286 eV in the high resolution XPS of C1s (Figure 15) confirms the presence of the amine functionalized ionic liquid (IL-NH_2) after all the catalysts were washed[55]. The amount of ionic liquid in the (0.1 wt. % IL-RGO)-TiO_2 sample is so small that the instrument is not able to detect and quantify the N1 atomic percent from the amine group (Table 10).

Table 10. Atomic percent concentration obtained by X-ray photoelectron spectroscopy (XPS)

Catalyst	**Atomic % Ti 2p**	**Atomic % C1**	**Atomic % O1**	**Atomic % N1**
RGO-TiO_2	15.91	32.46	51.63	0
(0.1 wt.% IL-RGO)-TiO_2	26.47	9.92	63.61	0
(0.2 wt.% IL-RGO)-TiO_2	25.77	10.65	63.37	0.21
(0.3 wt.% IL-RGO)-TiO_2	25.74	11.02	62.64	0.60
IL-RGO(reduced for 12 hours)-TiO_2	25.01	14.08	60.32	0.59
IL-RGO(reduced for 24 hours)-TiO_2	23.87	15.45	59.61	1.08
IL-RGO(reduced for 48 hours)-TiO_2	21.43	21.11	55.96	1.50
IL-RGO(reduced for 62 hours)-TiO_2	20.04	24.94	53.17	1.85
IL-RGO	0	80.73	12.72	6.55
GO	0	74.81	25.19	0

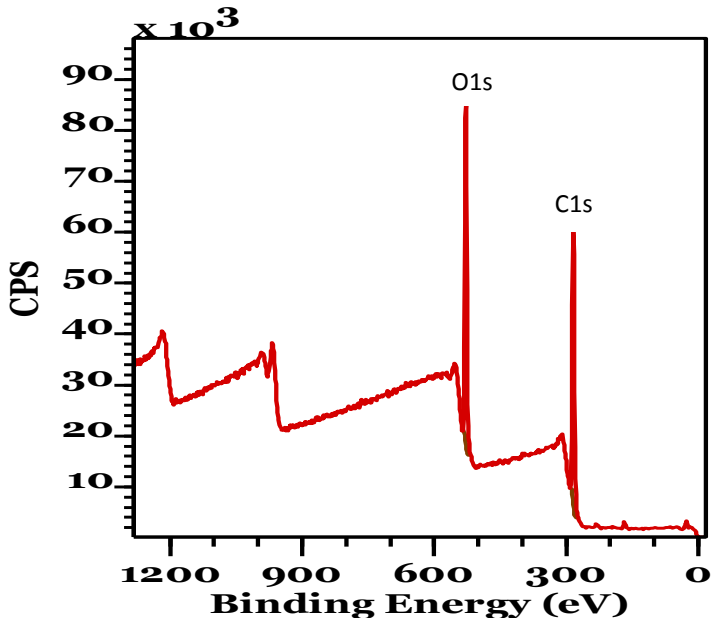

Figure 11. X-ray photoelectron spectroscopy (XPS) wide scan of graphite oxide (GO). The wide scan survey of GO showed the anticipated elements, which are oxygen and carbon

---

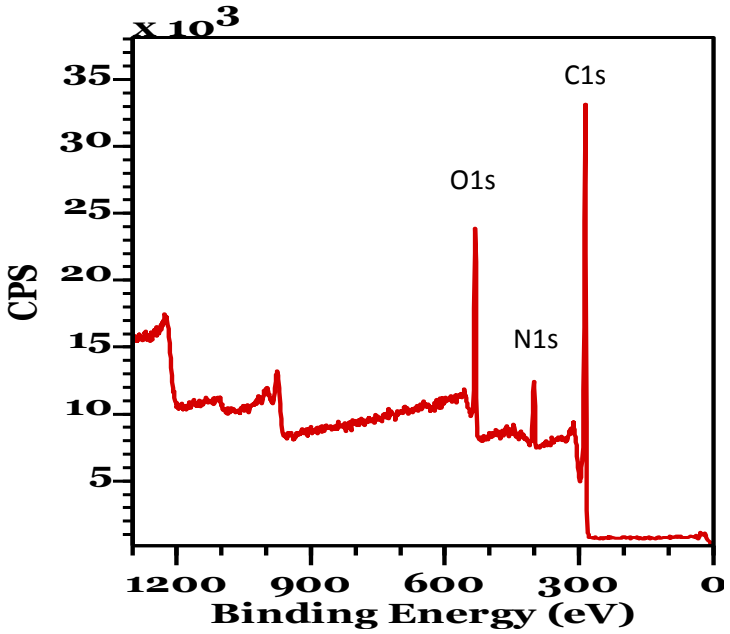

Figure 12. X-ray photoelectron spectroscopy (XPS) wide scan of the ionic liquid functionalized reduced graphite oxide (IL-RGO). The wide scan survey of the IL-RGO showed the anticipated elements, which are oxygen, carbon, and nitrogen

---

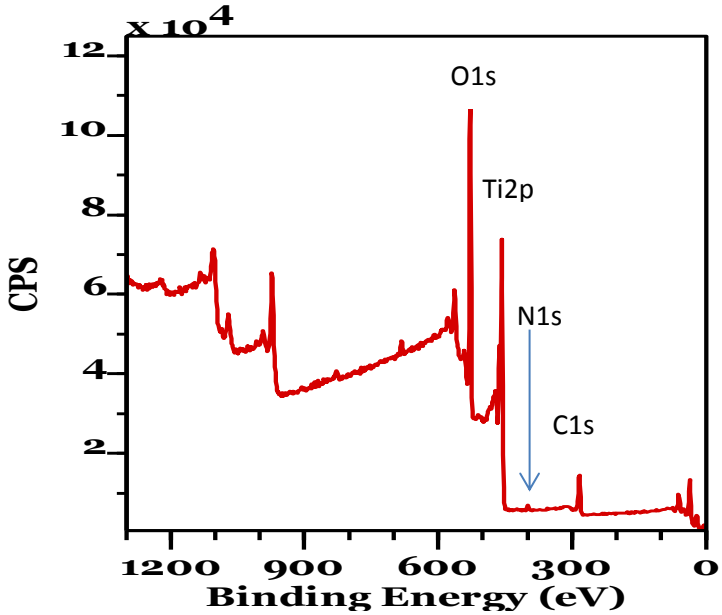

Figure 13. X-ray photoelectron spectroscopy (XPS) wide scan of the ionic liquid functionalized reduced graphite oxide-TiO_2 (IL-RGO-TiO_2). The wide scan survey of the IL-RGO-TiO_2 showed the anticipated elements, which are oxygen, carbon, nitrogen, and titanium

---

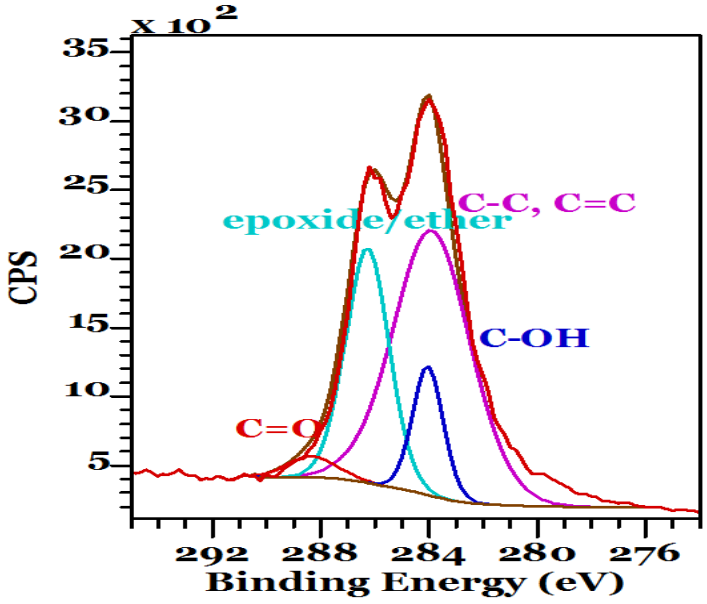

Figure 14. X-ray photoelectron spectroscopy (XPS) high resolution spectrum of C1s in graphite oxide (GO). The high resolution spectrum of C1 in GO showed that the carbon peak is comprised of different binding configurations C=C, C-C, C=O, C-OH, and epoxide/ether

---

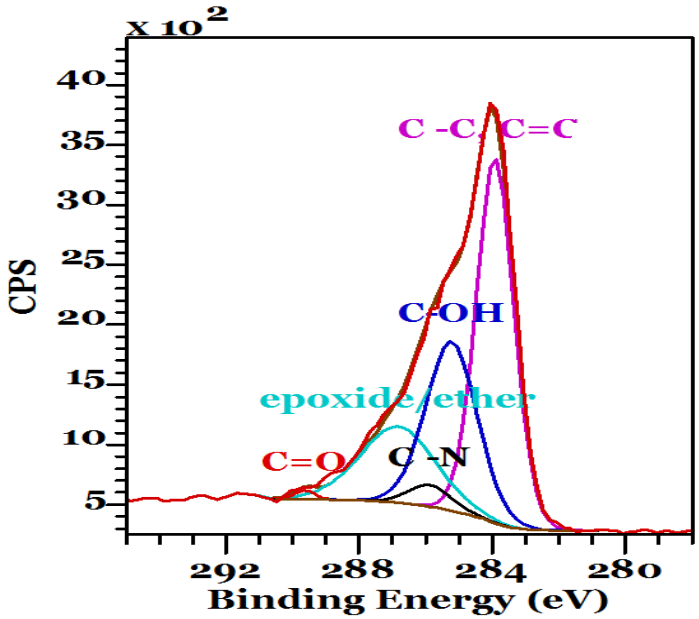

Figure 15. X-ray photoelectron spectroscopy (XPS) high resolution spectrum of C1s in the ionic liquid functionalized reduced graphite oxide (IL-RGO). The high resolution spectrum of C1 in the IL-RGO demonstrated the reduction of the epoxide/ether bonds, which occurred when GO was reacted with KOH and NH_2-C_4mimCl in the presence of heat

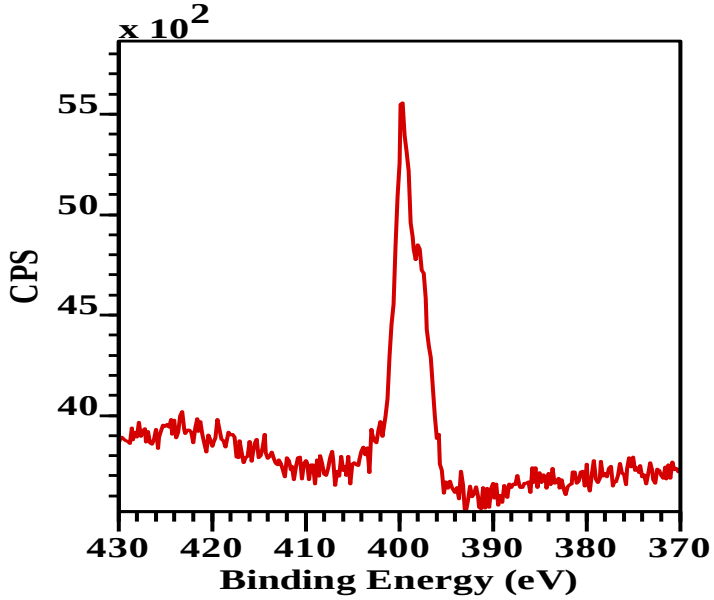

Figure 16. X-ray photoelectron spectroscopy (XPS) high resolution spectrum of N1s in the ionic liquid functionalized reduced graphite oxide (IL-RGO). The high resolution spectrum of N1 in IL-RGO confirms the presence of the ionic liquid (IL-NH_2)

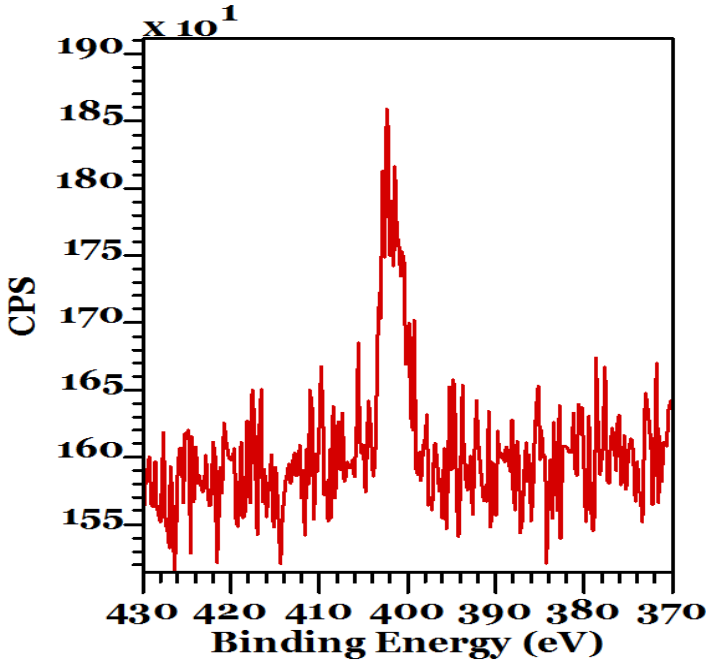

Figure 17. X-ray photoelectron spectroscopy (XPS) high resolution spectrum of N1s in the ionic liquid functionalized reduced graphite oxide-TiO_2 (IL-RGO-TiO_2). The high resolution spectrum of N1 in IL-RGO-TiO_2 confirms the presence of the ionic liquid (IL-NH_2) after the catalyst was washed

---

UV-vis absorbance spectra of the synthesized RGO-TiO_2, IL-RGO-TiO_2 catalysts, and commercial TiO_2 were acquired. The results are presented in Figures 18, 19, 20, and 21. All of the absorption edges for the catalyst overlap with commercial TiO_2. Thus, there was not a significant change in the bandgap energy for the catalysts, which is consistent with literature[69].

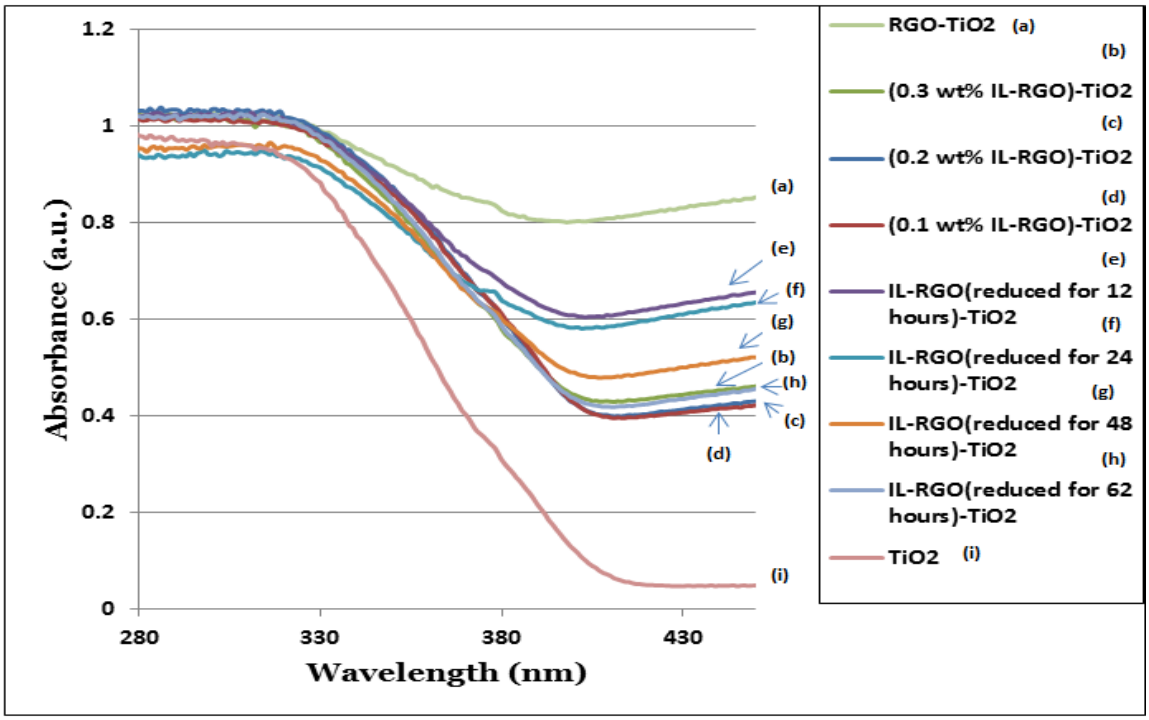

Figure 18. UV-vis absorbance spectra for all IL-RGO-TiO_2, commercial TiO_2, and RGO-TiO_2 composites

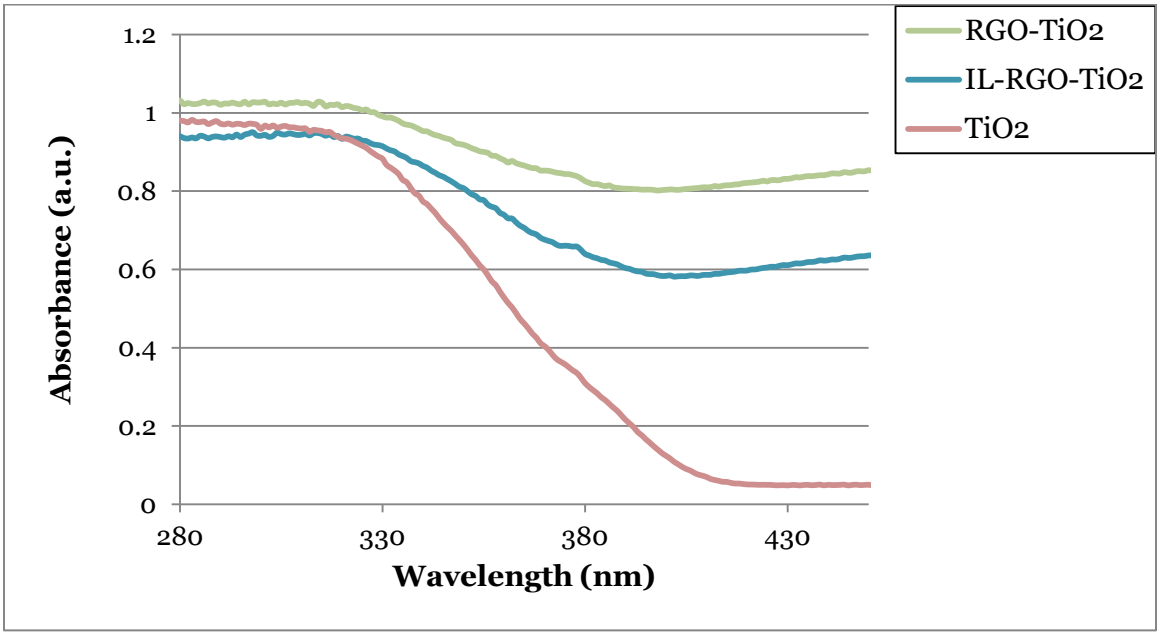

Figure 19. UV-vis absorbance spectra for IL-RGO-TiO_2, commercial TiO_2, and RGO-TiO_2

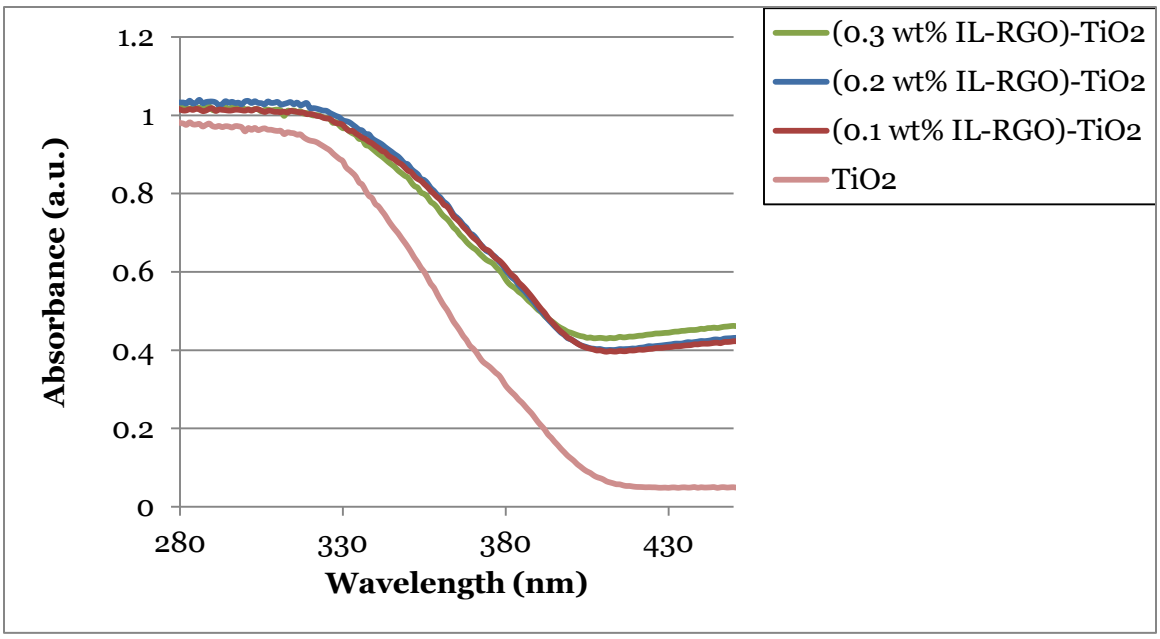

Figure 20. UV-vis absorbance spectra for IL-RGO-TiO_2 with different weight percentages

---

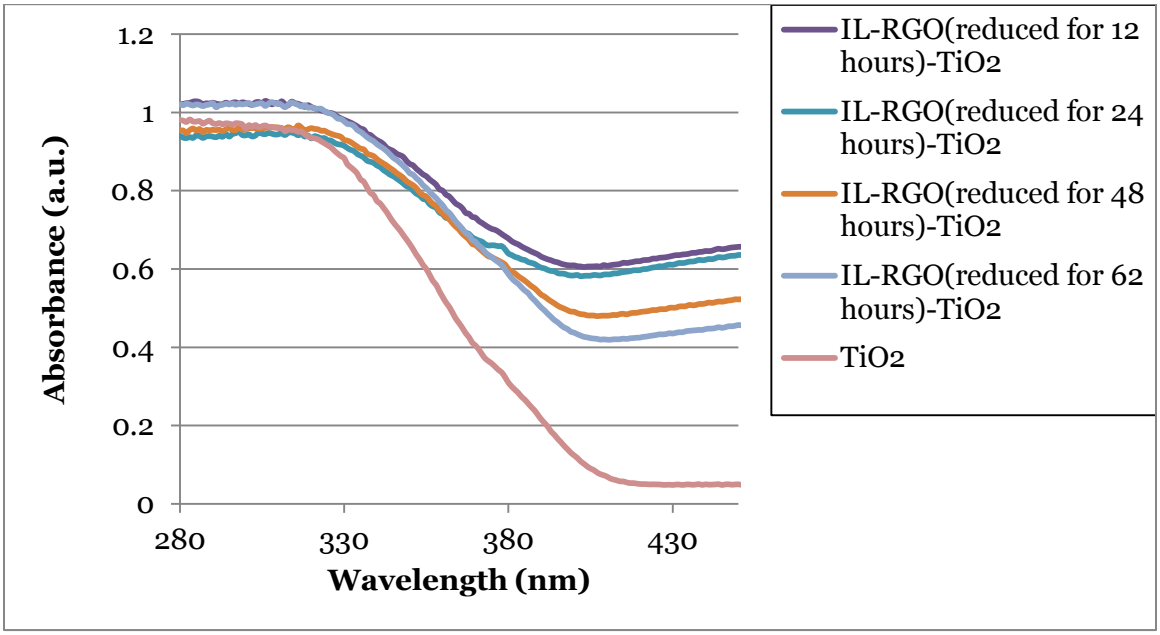

Figure 21. UV-vis absorbance spectra for IL-RGO-TiO_2 samples where the IL-RGO was reduced for different periods of time

---

Table 11 illustrates the estimated bandgap energy values for all of the catalyst that were synthesized. Estimated bandgap energies were found by recording the cut off wavelength (λ), which is the point where the absorbance value is minimum, and the equation described in Table 11 [70-72]. The results indicate that the commercial TiO_2 bandgap energy is about 3.05 eV whereas the IL-RGO-TiO_2 and RGO-TiO_2 bandgap energies indicate slightly larger values ranging between 3.08eV-3.19eV, however still an insignificant change when compared to the bandgap energy of commercial TiO_2. As mentioned earlier in this document, all the bandgap energies are about the same since the absorption edge overlaps. The overlap of the absorption edge has to do with the color of the catalyst (light gray for IL-RGO-TiO_2 and dark gray for RGO-TiO_2), size of the particles and defects on the surface[70, 73].

Table 11. Estimated bandgap energies for each of the catalysts

Catalyst	**λ = Cut off wavelength (m)**	**Bandgap energy[A] (eV)**
RGO-TiO_2	3.90E-07	3.19
(0.1 wt.% IL-RGO)-TiO_2	4.04E-07	3.08
(0.2 wt.% IL-RGO)-TiO_2	4.03E-07	3.08
(0.3 wt.% IL-RGO)-TiO_2	4.01E-07	3.10
IL-RGO(reduced for 12 hours)-TiO_2	3.92E-07	3.17
IL-RGO(reduced for 24 hours)-TiO_2	3.93E-07	3.16
IL-RGO(reduced for 48 hours)-TiO_2	3.99E-07	3.11
IL-RGO(reduced for 62 hours)-TiO_2	3.99E-07	3.11
TiO_2	4.07E-07	3.05

[A]The value of the bandgap energy (E) was calculated using the equation (E) = h*C/λ. Planks constant (h) = 6.626 x 10^{-34} Joules.sec and speed of light (C) = 3.0x10^8 meter/sec. Where 1eV = 1.6X10^{-19} joules (conversion factor)

Brunauer–Emmett–Teller (BET) results are presented in Table 12. Table 12 demonstrates that there was a surface area increase by modifying TiO_2 with the IL-RGO. The surface area data establishes an almost insignificant change when using different weight percentages of IL-RGO ranging from 0.1-0.3 wt. %, however there is a significant variation in surface area when the reduction time of IL-RGO increases. The reduction time of 48 hours seems to represent the point at which the surface area (58.6 ± 3.0 m^2/g) is at its highest, and then the surface area decreases, meaning that a possible ionic liquid decomposition is occurring leading to a carbon to carbon sheet recombination (graphite particles are being created). The carbon sheet recombination should decrease the conductivity of the material, which represents a negative effect in the photocatalytic properties of the catalyst. During the washing step of the synthesis of RGO-TiO_2, there was a significant amount of TiO_2 lost. On the other hand, when synthesizing the IL-RGO-TiO_2 there was an insignificant amount of TiO_2 lost, thus the reason for the higher surface area of RGO-TiO_2 (63.5 ± 3.3m^2/g) as compared to any of the other catalyst used was due to the much higher amount of RGO in the catalyst.

Table 12. Brunauer–Emmett–Teller (BET) surface area results

Catalyst	**BET, surface area (m^2/g)**
RGO-TiO_2	63.5 ±3.3
(0.1 wt.% IL-RGO)-TiO_2	59.7 ±3.0
(0.2 wt.% IL-RGO)-TiO_2	58.8 ±3.0
(0.3 wt.% IL-RGO)-TiO_2	58.4 ±3.0
IL-RGO(reduced for 12 hours)-TiO_2	48.8 ±2.0
IL-RGO(reduced for 24 hours)-TiO_2	53.6 ±2.0
IL-RGO(reduced for 48 hours)-TiO_2	58.6 ±3.0
IL-RGO(reduced for 62 hours)-TiO_2	54.8 ±2.0
TiO_2	45.7 ±2.0

Photocatalysis Results

Photocatalytic Reduction of Carbon Dioxide in the Presence of Water Vapor Using an Ionic liquid Reduced Graphite Oxide-TiO_2 (IL-RGO-TiO_2) Composite versus Commercial TiO_2

Initial experiments were conducted to test the hypothesis that modifying TiO_2 with a highly conductive material like IL-RGO enhances the formation of products. Researchers have hypothesized that pretreatment of TiO_2 at high temperatures creates oxygen vacancies that enhances CO_2 reduction[32]. Thus, some of the commercial TiO_2 and IL-RGO-TiO_2 catalysts were pretreated in an effort to improve the production of products by creating oxygen vacancies in the TiO_2. The production of CO from the photocatalytic reduction of CO_2 in the presence of H_2O using untreated and pretreated IL-RGO-TiO_2 and TiO_2 is presented in Figure 22.

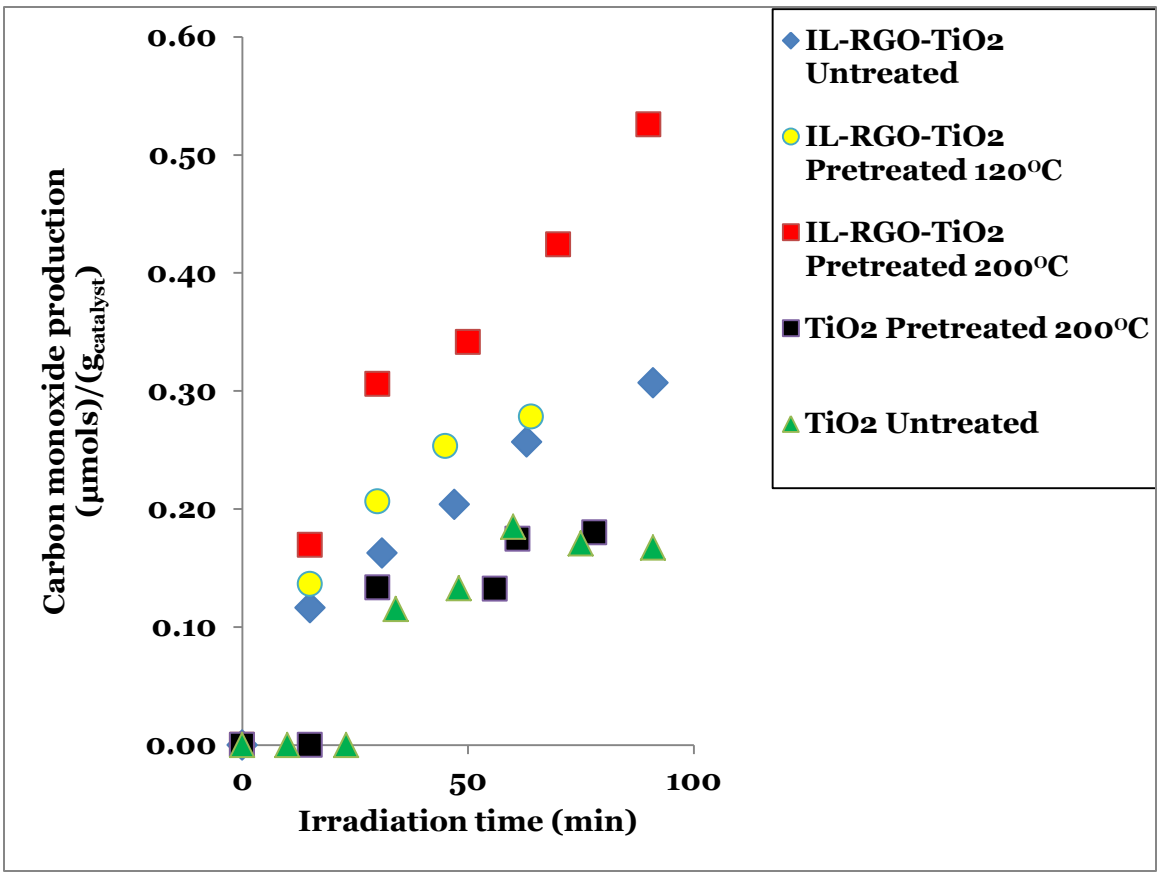

Figure 22. Carbon monoxide results from the photocatalytic conversion of carbon dioxide in the presence of water vapor over various untreated and pretreated IL-RGO-TiO_2 and TiO_2 catalysts, ± 1.87% error of the value

---

Carbon monoxide and CH_4 were the principal products formed and detected by the GC. The results of the CO production clearly showed that IL-RGO-TiO_2 (pretreated and untreated) had a higher photocatalytic CO production as compared to commercial TiO_2 (pretreated and untreated) over 90 minutes of UV light irradiation. The highest production observed was 0.41 µmol($g_{catalyst}$-hour)$^{-1}$ for IL-RGO-TiO_2 pretreated at 200^{O}C and 0.18 µmol($g_{catalyst}$-hour)$^{-1}$ for commercial TiO_2 pretreated at 200^{O}C.

It was clear that photocatalytic reactions occurred more efficiently when the catalyst was pretreated at high temperatures. The higher CO production using IL-RGO-TiO_2 versus commercial TiO_2 could be attributed to three factors: oxygen vacancies

generated on the TiO_2 surface by the pretreatment, the CO_2 attraction properties of the ionic liquid and the conductive properties of the RGO. No CO product was detected in the absence of the catalysts, meaning that the reactor was clean and that the reaction could not be initiated without the catalyst. No CO product was detected under dark conditions, signifying that the CO was produced through reaction that was initiated by UV light illumination. There was also no production of CO when running the same experiment in the absence of CO_2 or H_2O as the reactant. Thus, CO was produced by CO_2 conversion.

The results also indicated trace production of CH_4 for all of the catalysts. Based on the results, an untreated IL-RGO-TiO_2 (0.019 $\mu mol(g_{catalyst}\text{-}hour)^{-1}$) seemed to be a superior photocatalyst for the production of CH_4 as compared to 200^{O}C pretreated IL-RGO-TiO_2 (0.010 $\mu mol(g_{catalyst}\text{-}hour)^{-1}$), 120^{O}C pretreated IL-RGO-TiO_2 (0.010 $\mu mol(g_{catalyst}\text{-}hour)^{-1}$) and 200^{O}C pretreated TiO_2 (0.009 $\mu mol(g_{catalyst}\text{-}hour)^{-1}$). The small production of CH_4 could be attributed to different phenomena. Since CO is also a precursor for CH_4 formation, the amount of CH_4 produced could have been limited by the amount of CO produced. Finally, it is possible that a hole scavenger was needed in order to have more electrons available for the hypothesized eight electron reaction that may be needed to convert CO_2 and H_2O to CH_4 (as compared to the two electron reaction that is hypothesized for CO production).

Photocatalytic Reduction of Carbon Dioxide in the Presence of Water Vapor and Methanol as a Hole Scavenger Using an Ionic Liquid Reduced Graphite Oxide-TiO_2 (IL-RGO-TiO_2) Composite and Commercial TiO_2

Researchers have hypothesized that a hole scavenger such as methanol enhances the production of products by inhibiting electro/hole recombination[74]. Thus, a similar

approach was undertaken to enhance CO_2 photocatalytic reduction to fuels. The production results of CO from the conversion of CO_2 in the presence of H_2O and methanol over various pretreated (200^oC) IL-RGO-TiO_2 and TiO_2 catalysts are presented in Figure 23.

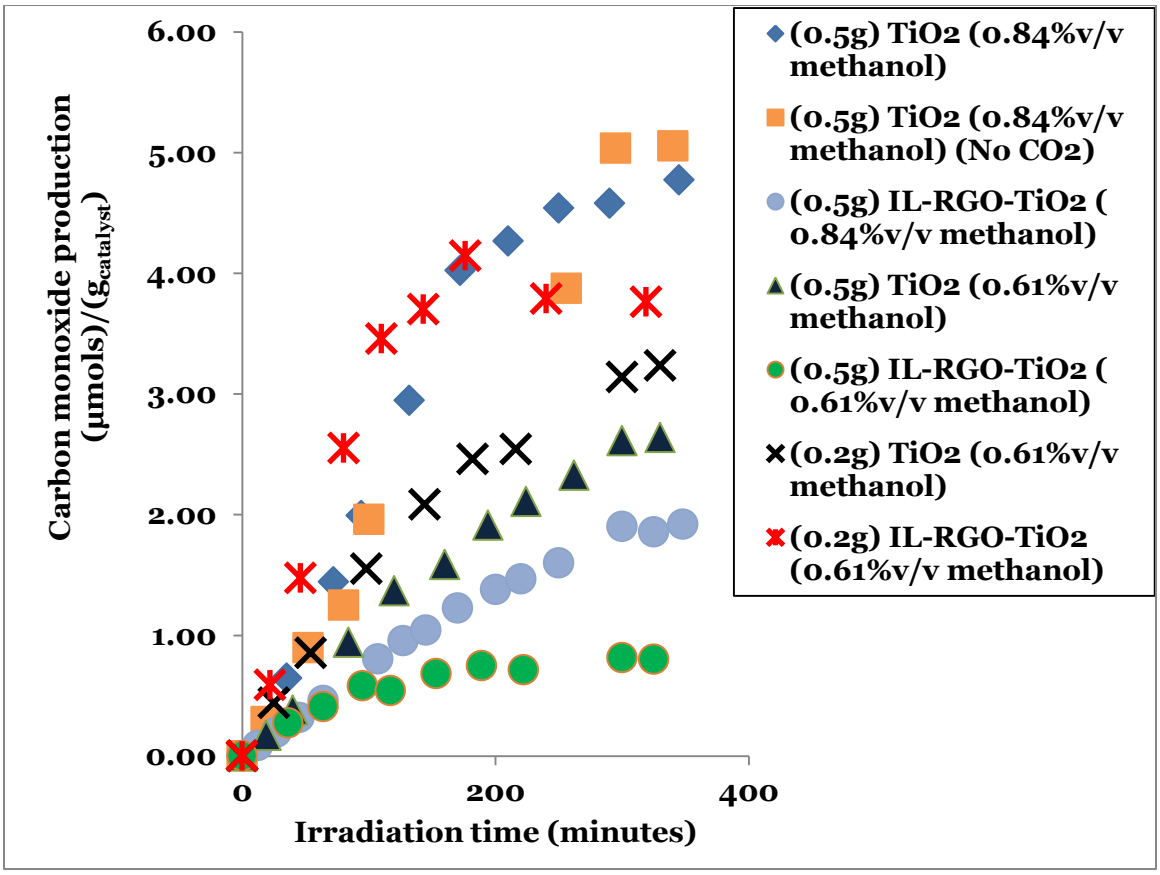

Figure 23. Carbon monoxide results from the photocatalytic conversion of carbon dioxide in the presence of water vapor and methanol as a hole scavenger over various pretreated (200^oC) IL-RGO-TiO_2 and TiO_2 catalysts, ± 1.87% error of the value.

Carbon monoxide and CH_4 were the principal products formed and detected by the GC. The results indicated that (0.2g) IL-RGO-TiO_2 (0.61%v/v methanol) and (0.5g) TiO_2 (0.84%v/v methanol) revealed a CO production of 1.41 and 1.02 µmol($g_{catalyst}$-hour)$^{-1}$

respectively over 350 minutes of irradiation. The results for IL-RGO-TiO_2 reached its highest production faster as compared to commercial TiO_2, which represent the higher availability of holes in the IL-RGO-TiO_2 catalyst. The production rate was taken at the point in which the respective experiment revealed the higher CO production.

To verify the source of the CO that formed, a background experiment with just helium flowing through H_2O and methanol was performed. The product concentration data for these experiments indicated that the principal source of the CO was the oxidation of methanol. This conclusion was further reinforced because of the increase that was appreciated in the CO_2 concentration upon irradiation. Carbon dioxide is a byproduct of a methanol oxidation reaction.

The idea of adding the hole scavenger (methanol) was to increase the production of CH_4, but that did not happened. The higher production of CH_4 observed in the experiments was only 0.010 $\mu mol(g_{catalyst}\text{-}hour)^{-1}$ for (0.2g) IL-RGO-TiO_2 (0.61%v/v methanol) and 0.009 $\mu mol(g_{catalyst}\text{-}hour)^{-1}$ for (0.2g) TiO_2 (0.61%v/v methanol) after 350 minutes of UV light irradiation. The small production of CH_4 could be attributed to different phenomena. Since CO is a precursor for CH_4 formation, the amount of CH_4 produced could have been limited by the amount of CO produced. Any CH_4 that was produced could also have undergone a secondary reaction where it was rapidly oxidized to CO and CO_2. Materials manufacturing issues may also have played a role. Specifically the conductivity of the IL-RGO may not have been high enough to inhibit electron/hole recombination, thus a longer IL-RGO reduction time may have been needed in order to gain conductivity. Alternatively, the reduction time of IL-RGO was excessive, thus leading to a decrease in interlayer spacing. This would make it difficult for the TiO_2 to deposit within the surface layers of the IL-RGO, thus adversely affecting charge separation for the production of CH_4.

Photocatalytic Reduction of Carbon Dioxide in the Presence of Water Vapor Using the Ionic Liquid Reduced Graphite Oxide-TiO_2 (IL-RGO-TiO_2) Composite Containing IL-RGO Reduced for Different Periods of Time

It was hypothesized that reducing the IL-RGO for different periods of time would enhance the photocatalytic properties of the IL-RGO-TiO_2 composite for the photocataytic reduction of CO_2 to fuels in the presence of H_2O. There was a possibility that 24 hours was not enough time to gain conductivity high enough to inhibit electron/hole recombination. Alternatively, there was a possibility that reducing the IL-RGO for 24 hours was an excessive time leading to a decrease in interlayer space that made it difficult for the TiO_2 to deposit on the surface of the IL-RGO, thus adversely affecting charge separation for the production of products. Thus, IL-RGO-TiO_2 composites were synthesized having IL-RGO reduced for 12, 48 and 62 hours. The production of CO from the photocatalytic reduction of CO_2 in the presence of H_2O using untreated IL-RGO-TiO_2 composites containing IL-RGO reduced at different periods of time are presented in Figure 24. As previously described, the experiments were conducted in a batch reactor.

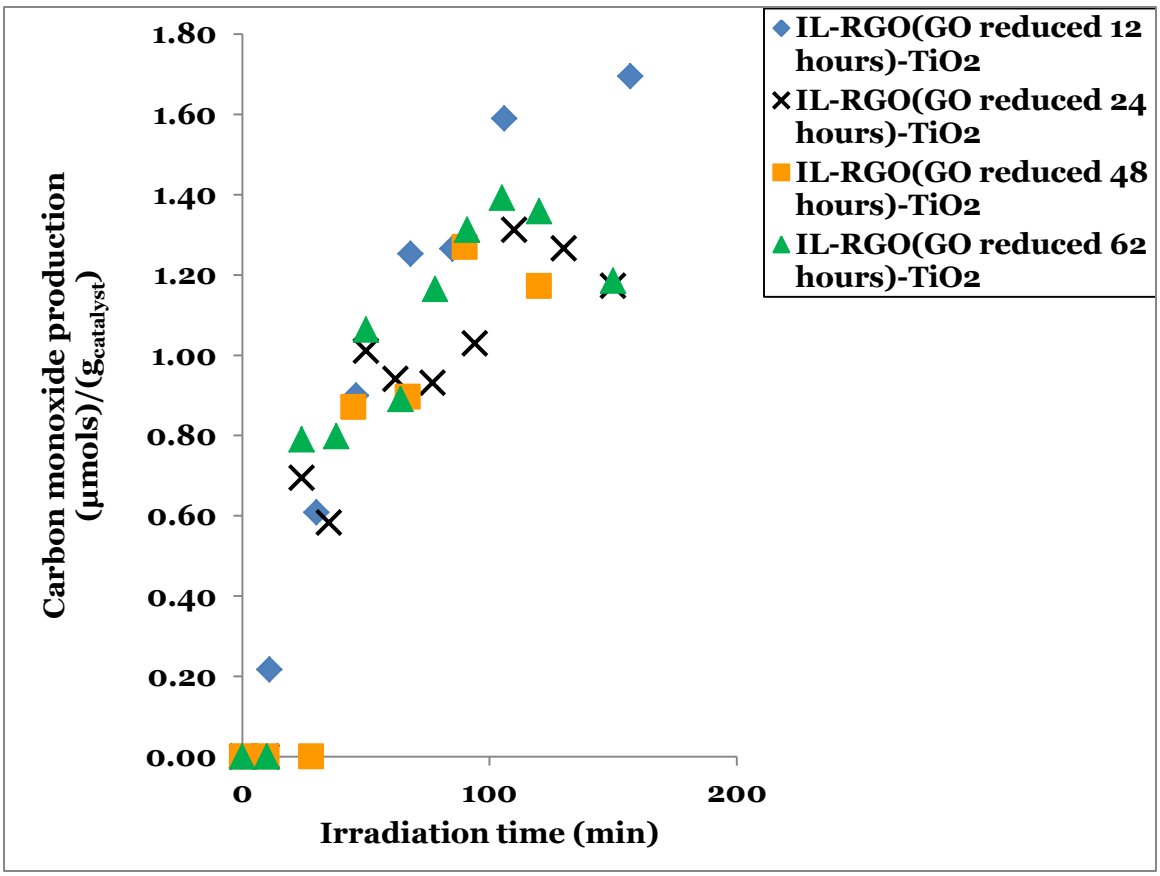

Figure 24. Carbon monoxide results from the photocatalytic conversion of carbon dioxide in the presence of water vapor over various untreated IL-RGO-TiO_2 catalysts with the IL-RGO reduced at different periods of time, ± 1.87% error of the value

---

Carbon monoxide and CH_4 were the principal products formed and detected by the GC. There was a slightly higher production of 0.65 µmol($g_{catalyst}$-hour)$^{-1}$ of CO at about 157 minutes of irradiation by using an IL-RGO reduced for 12 hours, but in general there were no significant differences. The rest of the catalysts exhibited a production rate of about 0.50 µmol($g_{catalyst}$-hour)$^{-1}$ after 150 minutes of irradiation. The results presented a maximum value that started to occur after 100 minutes of irradiation. The maximum value could represent a couple of things: (a) one of the reactants was limited in concentration, or (b) CO was consumed rapidly after being formed. No CO product was detected in the absence of the catalysts, indicating that the reactor was clean and that the

reaction could not be initiated without the catalyst. Carbon monoxide was not detected under dark conditions, i.e. the absence of UV light illumination. There was no production of CO when running the same experiment in the absence of CO_2 or H_2O. Thus, CO was produced by CO_2 photocatalytic reaction.

The results also indicated trace production of CH_4 for all of the catalysts. Methane production seemed to reach its highest point very rapidly. Based on these results an IL-RGO (GO reduced for 12 hours)-TiO_2 catalyst basically had the same CH_4 production rate (0.040 $\mu mol(g_{catalyst}\text{-hour})^{-1}$) as compared to IL-RGO (GO reduced for 62 hours-TiO_2 (0.035 $\mu mol(g_{catalyst}\text{-hour})^{-1}$). The CH_4 production was negligible in all experiments, suggesting that a change in the IL-RGO reduction times did not have an appreciable effect on CH_4 formation. The small production of CH_4 could be attributed to different phenomena. Since CO is also a precursor for CH_4 formation, the amount of CH_4 produced could have been limited by the amount of CO produced. Finally, there was a possibility that the attachment of the ionic liquid was negatively affecting the conductivity of the RGO, thus not enough electrons were available for CO_2 reduction.

Photocatalytic Reduction of Carbon Dioxide in the Presence of Water Vapor Using an Ionic Liquid Reduced Graphite Oxide-TiO_2 (IL-RGO-TiO_2) Composite and a Reduced Graphite Oxide-TiO_2 (RGO-TiO_2) Composite

A set of experiments were conducted to test if the attachment of the ionic liquid to the reduced graphite oxide negatively affects the photocatalytic formation of products when using IL-RGO-TiO_2 for the photocatalytic reduction of CO_2 in the presence of H_2O. The production of CO from the photocatalytic reduction of CO_2 in the presence of H_2O using untreated IL-RGO-TiO_2 and RGO-TiO_2 are presented in Figure 25.

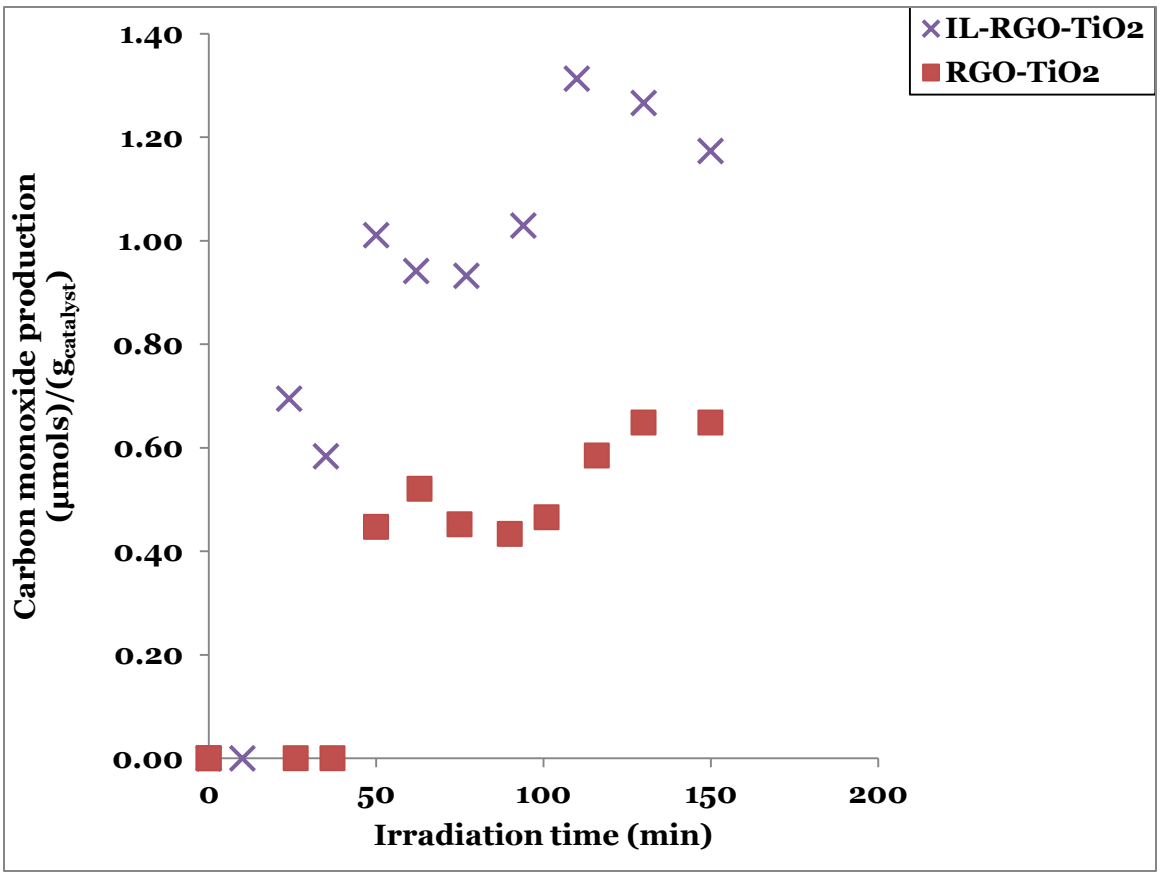

Figure 25. Carbon monoxide results from the photocatalytic conversion of carbon dioxide in the presence of water vapor over untreated IL-RGO-TiO_2 and RGO-TiO_2, ± 1.87% error of the value

---

Carbon monoxide and CH_4 were the principal products formed and detected by the GC. It was clear that there was a superior production of CO (0.72µmol($g_{catalyst}$-hour)$^{-1}$) when using an IL-RGO-TiO_2 composite as compared to using RGO-TiO_2 (0.30 µmol($g_{catalyst}$-hour)$^{-1}$). Furthermore, the production of CO when using IL-RGO-TiO_2 occurred faster as compared to RGO-TiO_2. The fact that it took at least 20 minutes for the CO to start producing when using IL-RGO-TiO_2 represents a potential condition in which a compound that was not detected by the current GC, e.g. HCOOH, decomposed to CO.

The higher and faster production of CO when using IL-RGO-TiO_2 could be due to the properties of the ionic liquid. The ionic liquid would help to attract the CO_2 to the surface of the catalyst. Thus, there will be more CO_2 molecules to react with the excited electrons resulting in higher and faster amounts of products as compared to just RGO-TiO_2. No CO product was detected in the absence of the catalysts, meaning that the reactor was clean and that the reaction could not initiate without the catalyst. No CO product was detected under dark conditions, meaning that it was only produced catalytically under UV light illumination. There was also no production of CO when running the same experiment in the absence of CO_2 or H_2O. Thus, CO was produced only by CO_2 conversion.

The results also indicated trace production of CH_4 for both of the catalysts, however it seemed to reach its maximum production very rapidly. Results demonstrated that an IL-RGO-TiO_2 and RGO-TiO_2 had the same production of 0.02μmol($g_{catalyst}$-hour)$^{-1}$ of CH_4. The CH_4 production was minor in both experiments meaning the production of CH_4 was not being restricted by the attachment of the ionic liquid to the reduced graphite oxide. The small production of CH_4 could be attributed to different phenomena. Since CO is also a precursor for CH_4 formation, the amount of CH_4 produced could have been limited by the amount of CO produced. Also, the amount of IL-RGO in the IL-RGO-TiO_2 was probably too much, and since the theoretical conductivity of IL-RGO is so high most of the electrons were held by the IL-RGO, rather than allowing them to react with the CO_2.

Photocatalytic Reduction of Carbon Dioxide in the Presence of Water Vapor Using an Ionic Liquid Reduced Graphite Oxide-TiO_2 (IL-RGO-TiO_2) Composite With 0.3, 0.2, and 0.1 Weight Percent of IL-RGO

Experiments were conducted to determine if decreasing the amount of IL-RGO from ~2-5 weight percent to 0.1-0.3 weight percent in the IL-RGO-TiO_2 composite would enhance the photocatalytic production of products. The indicated hypothesis was tested because previous work suggests that a high concentration of the conductive material might be counterproductive for CO_2 photocatalytic reduction experiments, since too much of a conductive material might hold onto the electrons due to the absorbance of the RGO [48, 75]. The production of CO from the photocatalytic reduction of CO_2 in the presence of H_2O using different IL-RGO weight percentages in the IL-RGO-TiO_2 composite are presented in Figures 26.

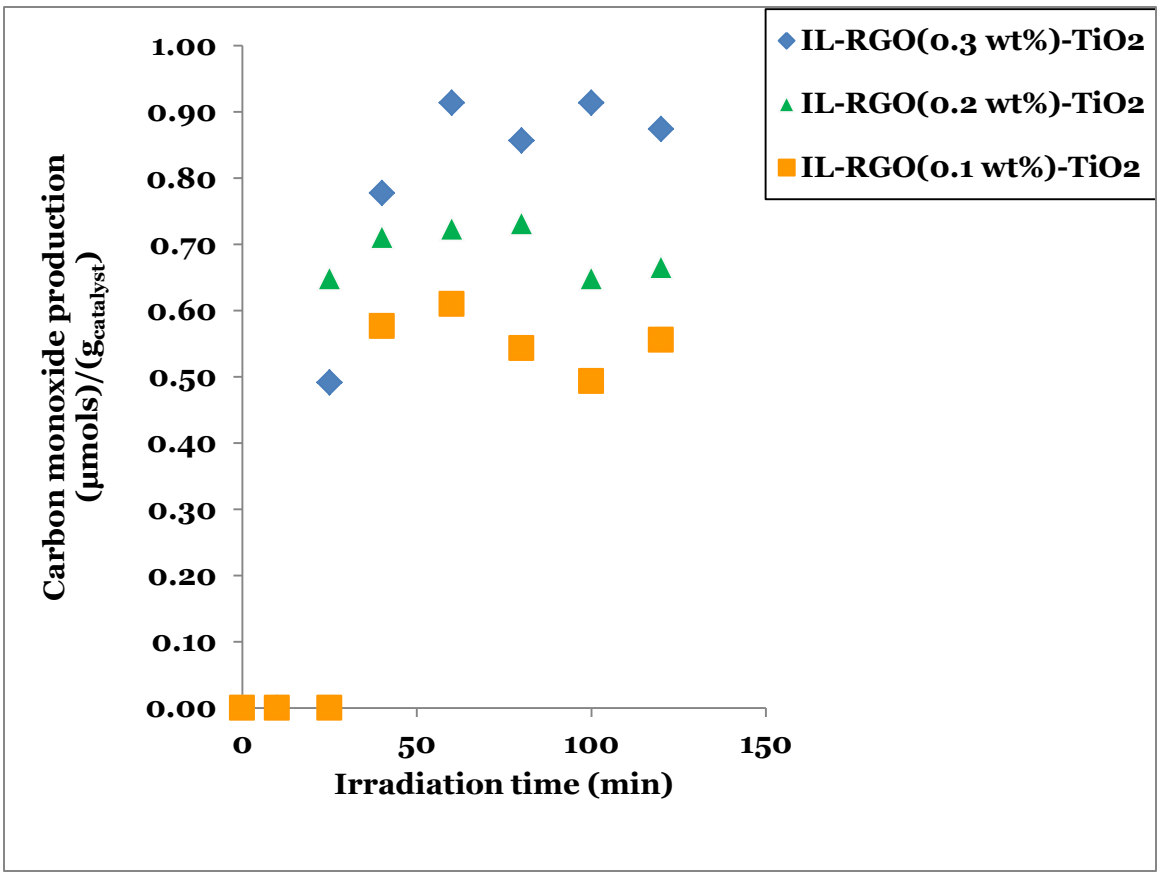

Figure 26. Carbon monoxide results from the photocatalytic conversion of carbon dioxide in the presence of water vapor over untreated IL-RGO-TiO_2 Containing different IL-RGO weight percentages, ± 1.87% error of the value

---

Carbon monoxide and CH_4 were the principal products formed and detected by the GC. The results showed insignificant CO photocatalytic production difference when comparing different low weight percentages (0.1, 0.2, and 0.3 wt. %) of IL-RGO in the IL-RGO-TiO_2 catalysts. The data illustrated that low levels of IL-RGO in the IL-RGO-TiO_2 material could decrease the product formation potential since less than 0.2 wt. % of IL-RGO did not present enough ionic liquid (as seen with the XPS data) to enhance the photocatalytic activity of the catalyst. The highest production of CO was 0.91 $\mu mol(g_{catalyst}\text{-hour})^{-1}$ obtained when using 0.3 wt. % IL-RGO-TiO_2. The catalysts

containing 0.2 wt. % and 0.1 wt. % IL-RGO resulted in a production of 0.72 and 0.60 $\mu mol(g_{catalyst}\text{-}hour)^{-1}$, respectively. No CO product was detected in the absence of the catalysts, meaning that the reactor was clean and that the reaction could not be initiated without the catalyst. No CO products were detected under dark conditions or in the absence of CO_2 and H_2O, thus indicating that CO was produced by CO_2 photoinduced catalytic conversion in the presence of H_2O.

The results in Figure 26 illustrated a plateau that starts to occur after 30 minutes of irradiation. The plateau signifies that a steady state production level was reached.

The results also indicated trace production of CH_4 for all of the catalysts, however it seemed to reach its highest point very rapidly. Results showed that there was a production of about 0.026 $\mu mol(g_{catalyst}\text{-}hour)^{-1}$ of CH_4 for all the catalyst. The CH_4 production was insignificant in these experiments, indicating that the production of CH_4 was not being restricted by the content of 1-3 wt. % IL-RGO. The small production of CH_4 could be attributed to different phenomena. Since CO is also precursor for CH_4 formation, the amount of CH_4 produced was limited by the CO produced. Another reason could be that not enough electrons were available for CO_2 conversion to CH_4.

CONCLUSIONS AND RECOMMENDATIONS

The photocatalytic activity for the reduction of CO_2 over a new carbon/semiconductor material in the presence of H_2O was investigated using a gas chromatograph (GC). The new photocatalytic material was a blend of a highly conductive surface (ionic liquid functionalized reduced graphite oxide (IL-RGO)) and a photocatalyst (TiO_2). The synthesis of the IL-RGO-TiO_2 was confirmed by Raman spectroscopy and X-ray photoelectron spectroscopy (XPS). An increase in surface area when modifying TiO_2 with the IL-RGO was confirmed by Brunauer–Emmett–Teller (BET) characterization. The estimated bandgap energies were examined using UV-vis absorbance spectra data. Gas chromatography results indicate that the ionic liquid functionalized reduced graphite oxide-TiO_2 composite was able to produced CO from the photocatalytic reduction of CO_2 in the presence of H_2O, but was unable to produce significant amounts of CH_4.

The IL-RGO-TiO_2 composite led to twice the production of CO from CO_2 conversion in comparison to unmodified TiO_2. The introduction of a commonly known hole scavenger such as methanol did not enhance the photocatalytic production of CH_4, but it did produce more CO as compared to any experiment conducted due to the oxidation of methanol. Different reduction times (during the reduction of graphite oxide step) of the IL-RGO did not have a significant impact on the photocatalytic production of CO and/or CH_4. It was demonstrated that there was twice CO production using ionic IL-RGO-TiO_2 as compared to RGO-TiO_2. This phenomenon was likely due to the enhanced attraction of CO_2 on the surface of the catalyst. However, the CH_4 production was about the same for both catalysts. The modification of different low IL-RGO weight percentages in the IL-RGO-TiO_2 composite did not lead to a substantial increase in CO

or CH_4 production. The maximum formation of products in each set of experiments is presented in Table 13.

Table 13: Major results obtained in the conversion of CO_2 in the presence of water over selected catalytic materials

Experiment name	Catalyst	Pretreatment conditions	Product formed	Product production $\mu mol(g_{catalyst}\text{-}hour)^{-1}$
IL-RGO-TiO_2 versus unmodified TiO_2	IL-RGO-TiO_2 TiO_2	200 °C	CO	0.41 0.18
IL-RGO-TiO_2 versus unmodified TiO_2	IL-RGO-TiO_2 TiO_2	Untreated 200 °C	CH_4	0.019 0.010
Methanol oxidation	IL-RGO-TiO_2 TiO_2	200 °C	CO	1.41 1.02
Methanol oxidation	IL-RGO-TiO_2 TiO_2	200 °C	CH_4	0.010 0.009
IL-RGO reduced at different times	IL-RGO(reduced 12 hours)-TiO_2	Untreated	CO	0.65
IL-RGO reduced at different times	IL-RGO(reduced 12 hours)-TiO_2	Untreated	CH_4	0.04
IL-RGO-TiO_2 versus RGO-TiO_2	IL-RGO-TiO_2 RGO-TiO_2	Untreated	CO	0.72 0.30
IL-RGO-TiO_2 versus RGO-TiO_2	IL-RGO-TiO_2 RGO-TiO_2	Untreated	CH_4	0.02 0.02
Different amounts of IL-RGO	IL-RGO(0.3wt%)-TiO_2	Untreated	CO	0.91
Different amounts of IL-RGO	IL-RGO(0.3wt%)-TiO_2	Untreated	CH_4	0.026

The work described demonstrates that an IL-RGO-TiO_2 is a novel and effective catalyst that boosts the production of CO in comparison to commercial TiO_2, due to the enhanced electron-hole separation and CO_2 attraction properties. In contrast, CH_4 production was not increased. XPS data reveal that all the catalysts had more than 1 atomic percent of carbon. Previous work suggests that an atomic concentration higher than 1 percent might be counterproductive for CO_2 photocatalytic reduction experiments, as too much of a conductive material might capture or hold onto the electrons due to the absorbance of the RGO[48, 75].

The chemical properties of this novel catalyst, the theoretical negligible environmental impact of the IL-RGO-TiO_2, and the results obtained suggest that there is a lot more photocatalytic potential to investigate, which could be the beginning of exceptional results for CO_2 photocatalytic reduction to higher value products. As mentioned earlier, Ti-based catalysts have shown promising results for CO_2 photocatalytic reduction, but the results still show low production amounts of the desired products (e.g. CH_4). Thus, the expansion to carbon nano-materials and ionic liquids to help enhance fuel production might be the next step that scientists could take.

Recommendations for future work are listed below.

1. Determine the conductivity of the IL-RGO. This will help to understand if the low production of photocatalytic products was due to unavailability of electrons for CO_2 reduction.
2. Determine the effect of the temperature used during the synthesis process on the hydrophobic and hydrophilic properties of the RGO. Past studies suggest that since GO and TiO_2 are hydrophilic whereas RGO is hydrophobic, as the reduction of GO increases the binding of IL-RGO and TiO_2 might be more

difficult[46]. Thus, producing a negative effect for charge separation within the IL-RGO-TiO_2 catalysts[46]. The results could help to understand if a different temperature is needed during the synthesis of the catalyst.

3. Determine the reaction mechanism of which the CO and CH_4 in this document were produced. This will help to understand if a potential condition in which a compound that was not detected by the current GC, e.g. HCOOH, decomposed to CO.

REFERENCES

[1] in Inventory of U.S. Greenhouse Gas Emissions and Sinks, Vol. (Ed.^Eds.: Editor), City, **1990-2012**.

[2] in Annual Energy Outlook 2013 with Projections to 2040, Vol. (Ed.^Eds.: Editor), City, **2013**.

[3] in Annual Energy Outlook 2014 Early Release Overview, Vol. (Ed.^Eds.: Editor), City, **2014**.

[4] in Advancing the Science of Climate Change, Vol. (Ed.^Eds.: Editor), National Research Council. The National Academies Press, City, **2012**.

[5] in **Annual Energy Review 2011**, Vol. (Ed.^Eds.: Editor), City, **2012**.

[6] in Inventory of U.S. greenhouse Gas Emissions and Sinks, Vol. (Ed.^Eds.: Editor), City, **1990-2011**.

[7] S. B. Wang, G. Q. M. Lu, G. J. Millar *Energy & Fuels*. **1996**, 10, 896-904.

[8] G. Centi, S. Perathoner *Catalysis Today*. **2009**, 148, 191-205.

[9] C. S. Song *Catalysis Today*. **2006**, 115, 2-32.

[10] B. Kumar, M. Llorente, J. Froehlich, T. Dang, A. Sathrum, C. P. Kubiak *Annual Review of Physical Chemistry, Vol 63*. **2012**, 63, 541-+.

[11] S. C. Roy, O. K. Varghese, M. Paulose, C. A. Grimes *Acs Nano*. **2010**, 4, 1259-1278.

[12] N. Serpone, E. Pelizzetti, photocatalysis fundamentals and applications, Wiley publishers, **1989**.

[13] U. I. Gaya, A. H. Abdullah *Journal of Photochemistry and Photobiology C-Photochemistry Reviews*. **2008**, 9, 1-12.

[14] D. S. Bhatkhande, V. G. Pangarkar, A. Beenackers *Journal of Chemical Technology and Biotechnology*. **2002**, 77, 102-116.

[15] F. Sastre, A. Corma, H. Garcia *Journal of the American Chemical Society*. **2012**, 134, 14137-14141.

[16] R. de Richter, S. Caillol *Journal of Photochemistry and Photobiology C-Photochemistry Reviews*. **2011**, 12, 1-19.

[17] E. E. Benson, C. P. Kubiak, A. J. Sathrum, J. M. Smieja *Chemical Society Reviews*. **2009**, 38, 89-99.

[18] L. Zhu, G. Shao, J. K. Luo *Semiconductor Science and Technology*. **2011**, 26.

[19] K. Ikeue, H. Yamashita, M. Anpo *Electrochemistry*. **2002**, 70, 402-408.

[20] M. Anpo, H. Yamashita, Y. Ichihashi, Y. Fujii, M. Honda *Journal of Physical Chemistry B*. **1997**, 101, 2632-2636.

[21] M. Anpo, H. Yamashita, K. Ikeue, Y. Fujii, S. G. Zhang, Y. Ichihashi, D. R. Park, Y. Suzuki, K. Koyano, T. Tatsumi *Catalysis Today*. **1998**, 44, 327-332.

[22] K. Ikeue, S. Nozaki, M. Ogawa, M. Anpo *Catalysis Letters*. **2002**, 80, 111-114.

[23] I. Keita, S. Nozaki, M. Ogawa, M. Anpo *Catalysis Today*. **2002**, 74, 241-248.

[24] Y. Shioya, K. Ikeue, M. Ogawa, M. Anpo *Applied Catalysis a-General*. **2003**, 254, 251-259.

[25] T. Inoue, A. Fujishima, S. Konishi, K. Honda *Nature*. **1979**, 277, 637-638.

[26] M. Ni, M. K. H. Leung, D. Y. C. Leung, K. Sumathy *Renewable & Sustainable Energy Reviews*. **2007**, 11, 401-425.

[27] K. Hashimoto, H. Irie, A. Fujishima *Japanese Journal of Applied Physics Part 1-Regular Papers Brief Communications & Review Papers*. **2005**, 44, 8269-8285.

[28] A. Heciak, A. W. Morawski, B. Grzmil, S. Mozia *Applied Catalysis B-Environmental*. **2013**, 140, 108-114.

[29] F. Akira, T. N, D. Rao, T. A *Journal of Photochemistry and Photobiology*. **2000**.

[30] U. Diebold *Surface Science Reports*. **2003**, 48, 53-229.

[31] M. Landmann, E. Rauls, W. G. Schmidt *Journal of Physics-Condensed Matter*. **2012**, 24.

[32] M. M. Rodriguez, X. H. Peng, L. J. Liu, Y. Li, J. M. Andino *Journal of Physical Chemistry C*. **2012**, 116, 19755-19764.

[33] M. Anpo, H. Yamashita, Y. Ichihashi, S. Ehara *Journal of Electroanalytical Chemistry*. **1995**, 396, 21-26.

[34] F. Saladin, L. Forss, I. Kamber *Journal of the Chemical Society-Chemical Communications*. **1995**, 533-534.

[35] K. Koci, L. Obalova, L. Matejova, D. Placha, Z. Lacny, J. Jirkovsky, O. Solcova *Applied Catalysis B-Environmental*. **2009**, 89, 494-502.

[36] G. H. Li, K. A. Gray *Chemical Physics*. **2007**, 339, 173-187.

[37] G. E. Brown, V. E. Henrich, W. H. Casey, D. L. Clark, C. Eggleston, A. Felmy, D. W. Goodman, M. Gratzel, G. Maciel, M. I. McCarthy, K. H. Nealson, D. A. Sverjensky, M. F. Toney, J. M. Zachara *Chemical Reviews*. **1999**, 99, 77-174.

[38] J. Mao, K. Li, T. Y. Peng *Catalysis Science & Technology*. **2013**, 3, 2481-2498.

[39] S. Teshome, R. Slva, C. Subrahmanyam *International Research Journal & Applied Chemistry*. **2011**.

[40] Z. Adriana *Recent Patents on Engineering*. **2008**.

[41] Y. T. Liang, B. K. Vijayan, K. A. Gray, M. C. Hersam *Nano Letters*. **2011**, 11, 2865-2870.

[42] D. H. Yoo, V. C. Tran, V. H. Pham, J. S. Chung, N. T. Khoa, E. J. Kim, S. H. Hahn *Current Applied Physics*. **2011**, 11, 805-808.

[43] A. Adan-Mas, D. Wei *Nanomaterials*. **2013**.

[44] T. Kuilla, S. Bhadra, D. H. Yao, N. H. Kim, S. Bose, J. H. Lee *Progress in Polymer Science*. **2010**, 35, 1350-1375.

[45] A. C. Neto, F. Guinea, N. M. R. Peres *Physics World*. **2006**, 19, 33-37.

[46] N. J. Bell, H. N. Yun, A. J. Du, H. Coster, S. C. Smith, R. Amal *Journal of Physical Chemistry C*. **2011**, 115, 6004-6009.

[47] Y. H. Ng, I. V. Lightcap, K. Goodwin, M. Matsumura, P. V. Kamat *Journal of Physical Chemistry Letters*. **2010**, 1, 2222-2227.

[48] W. Tu, Y. Zhou, Q. Liu, S. Yan, S. Bao, X. Wang, M. Xiao, Z. Zou *Advanced Functional Materials*. **2013**, 23, 1743-1749.

[49] W. G. Tu, Y. Zhou, Q. Liu, Z. P. Tian, J. Gao, X. Y. Chen, H. T. Zhang, J. G. Liu, Z. G. Zou *Advanced Functional Materials*. **2012**, 22, 1215-1221.

[50] Y. T. Liang, B. K. Vijayan, O. Lyandres, K. A. Gray, M. C. Hersam *Journal of Physical Chemistry Letters*. **2012**, 3, 1760-1765.

[51] W. J. Ong, M. M. Gui, S. P. Chai, A. R. Mohamed *Rsc Advances*. **2013**, 3, 4505-4509.

[52] X.-H. Xia, Z.-H. Jia, Y. Yu, Y. Liang, Z. Wang, L.-L. Ma *Carbon*. **2007**, 45, 717-721.

[53] N. I. Kovtyukhova, P. J. Ollivier, B. R. Martin, T. E. Mallouk, S. A. Chizhik, E. V. Buzaneva, A. D. Gorchinskiy *Chemistry of Materials*. **1999**, 11, 771-778.

[54] W. S. Hummers, R. E. Offeman *Journal of the American Chemical Society*. **1958**, 80, 1339-1339.

[55] H. F. Yang, C. S. Shan, F. H. Li, D. X. Han, Q. X. Zhang, L. Niu *Chemical Communications*. **2009**, 3880-3882.

[56] B. Y. Dai, L. Fu, L. Liao, N. Liu, K. Yan, Y. S. Chen, Z. F. Liu *Nano Research*. **2011**, 4, 434-439.

[57] M. Ramdin, T. W. de Loos, T. J. H. Vlugt *Industrial & Engineering Chemistry Research*. **2012**, 51, 8149-8177.

[58] T. T. Gao, J. M. Andino, J. R. Alvarez-Idaboy *Physical Chemistry Chemical Physics*. **2010**, 12, 9830-9838.

[59] J. F. Shen, M. Shi, B. Yan, H. W. Ma, N. Li, M. X. Ye *Nano Research*. **2011**, 4, 795-806.

[60] M. Halmann, V. Katzir, E. Borgarello, J. Kiwi *Solar Energy Materials*. **1984**, 10, 85-91.

[61] K. Adachi, K. Ohta, T. Mizuno *Solar Energy*. **1994**, 53, 187-190.

[62] K. R. Thampi, J. Kiwi, M. Gratzel *Nature*. **1987**, 327, 506-508.

[63] Z. Goren, I. Willner, A. J. Nelson, A. J. Frank *Journal of Physical Chemistry*. **1990**, 94, 3784-3790.

[64] in Operating Parameters for the Thermal Conductivity Detector in Varian 3800 and 3900 Gas Chromatographs, Vol. (Ed.^Eds.: Editor), Lotus flower, City, **2007**.

[65] in Analytical Laboratories Applications:GC with Flame Ionization Detector Vol. (Ed.^Eds.: Editor), Air products and chemicals, City, **2012**.

[66] T. N. Lambert, C. A. Chavez, B. Hernandez-Sanchez, P. Lu, N. S. Bell, A. Ambrosini, T. Friedman, T. J. Boyle, D. R. Wheeler, D. L. Huber *Journal of Physical Chemistry C*. **2009**, 113, 19812-19823.

[67] O. Akhavan, M. Abdolahad, A. Esfandiar, M. Mohatashamifar *Journal of Physical Chemistry C*. **2010**, 114, 12955-12959.

[68] S. Some, Y. Kim, Y. Yoon, H. Yoo, S. Lee, Y. Park, H. Lee *Scientific Reports*. **2013**, 3.

[69] B. Li, X. T. Zhang, X. H. Li, L. Wang, R. Y. Han, B. B. Liu, W. T. Zheng, X. L. Li, Y. C. Liu *Chemical Communications*. **2010**, 46, 3499-3501.

[70] V. Stengl, S. Bakardjieva, T. M. Grygar, J. Bludska, M. Kormunda *Chemistry Central Journal*. **2013**, 7.

[71] A. B. Murphy *Solar Energy Materials and Solar Cells*. **2007**, 91, 1326-1337.

[72] S. U. M. Khan, M. Al-Shahry, W. B. Ingler *Science*. **2002**, 297, 2243-2245.

[73] Q. Y. Zhang, T. T. Gao, J. M. Andino, Y. Li *Applied Catalysis B-Environmental*. **2012**, 123, 257-264.

[74] L. Liu, D. Pitts T, H. Zhao, C. Zhao, Y. Li in Silver- incorporated bicrystalline (anatase/brookite) TiO2 microspheres for CO2 photoreduction with wate in the presence of methanol, Vol. (Ed.^Eds.: Editor), Applied Catalyst, City, **2013**.

[75] Q. Zhang, T. Gao, J. M. Andino, Y. Li *Applied Catalysis B-Environmental*. **2012**, 123, 257-264.

APPENDIX

DATA COLLECTED 2012-2014

The process for operating the gas chromatographs was as follows. When starting the GC, a few runs using just the carrier gases were performed to clean the columns. Once the experiment in the photoreactor was ready and free of leaks, samples were taken manually from the septum port located in the top of the photoreactor using a 0.5mL Hamilton gas tight syringe. The syringe was previously flushed with an inert gas (N_2 or He) in order to eliminate any contamination.

The calibration curves were prepared by manually injecting to the GC the different gas concentrations and recording the peak area and retention time for each of the gases of interest. The gas concentrations were prepared in SKC Tedlar (1L) sample bags using a gas dilution technique. After each of the experiments finished, a point in each of the calibration curves was checked to make sure the retention time of each gas did not change and the peak areas were accurate. Examples of the calibration curves used to calculate the product concentrations are presented in Figures 27-30:

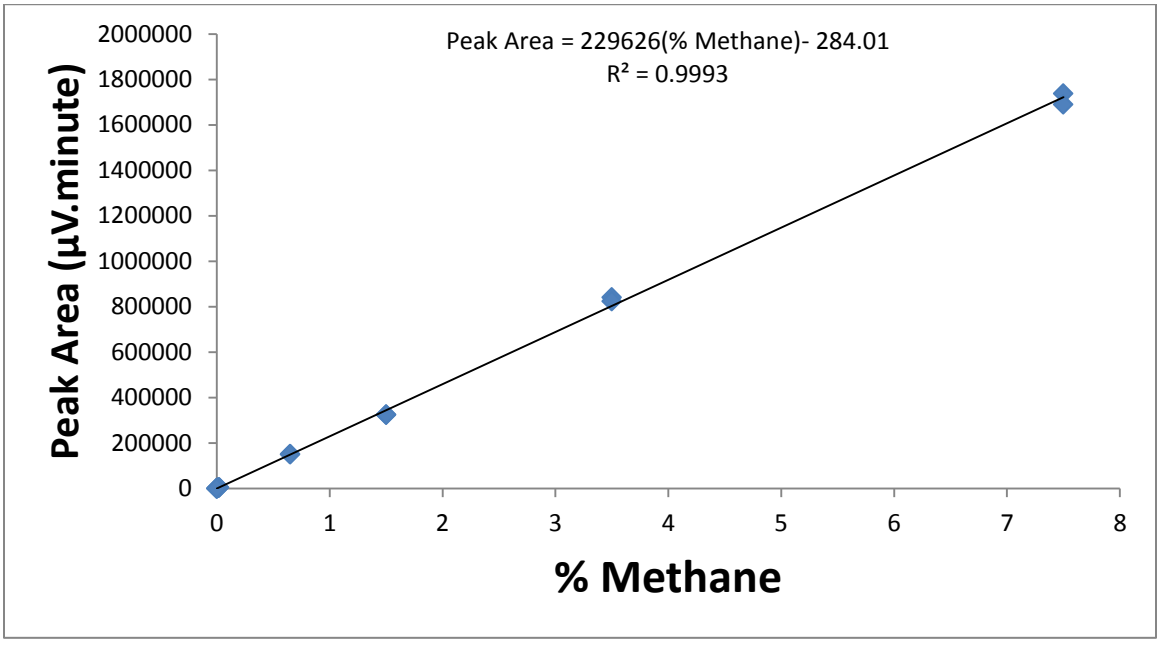

Figure 27. Calibration curve of methane, ± 3.20% error of the value

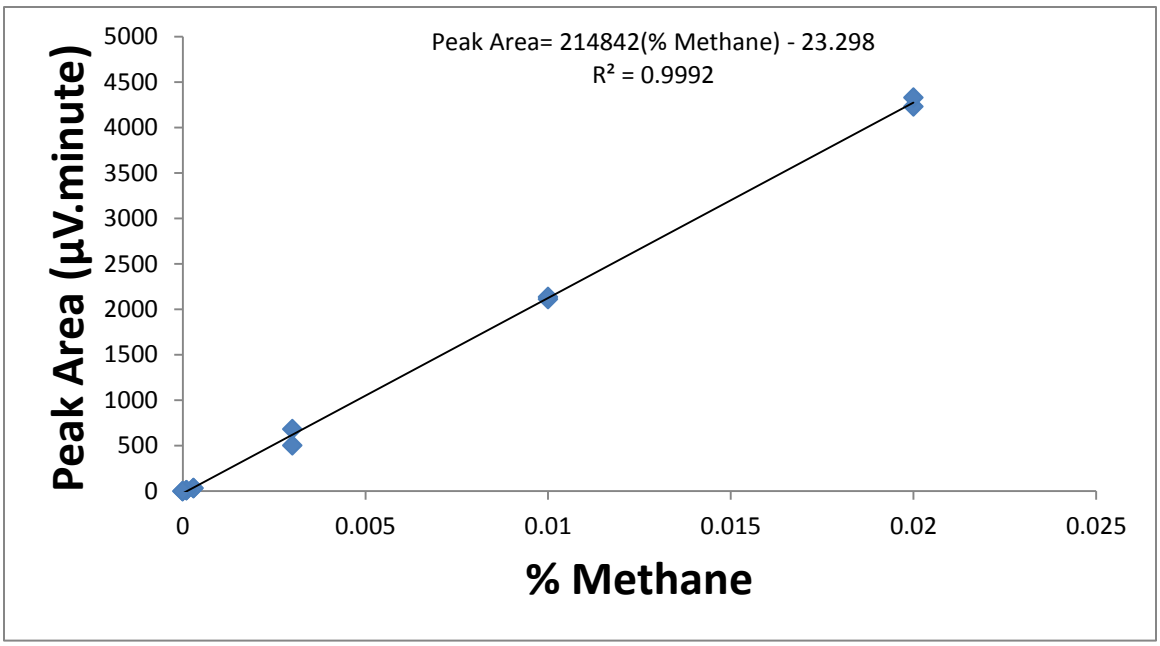

Figure 28. Calibration curve of methane (expanded), ± 3.20% error of the value

---

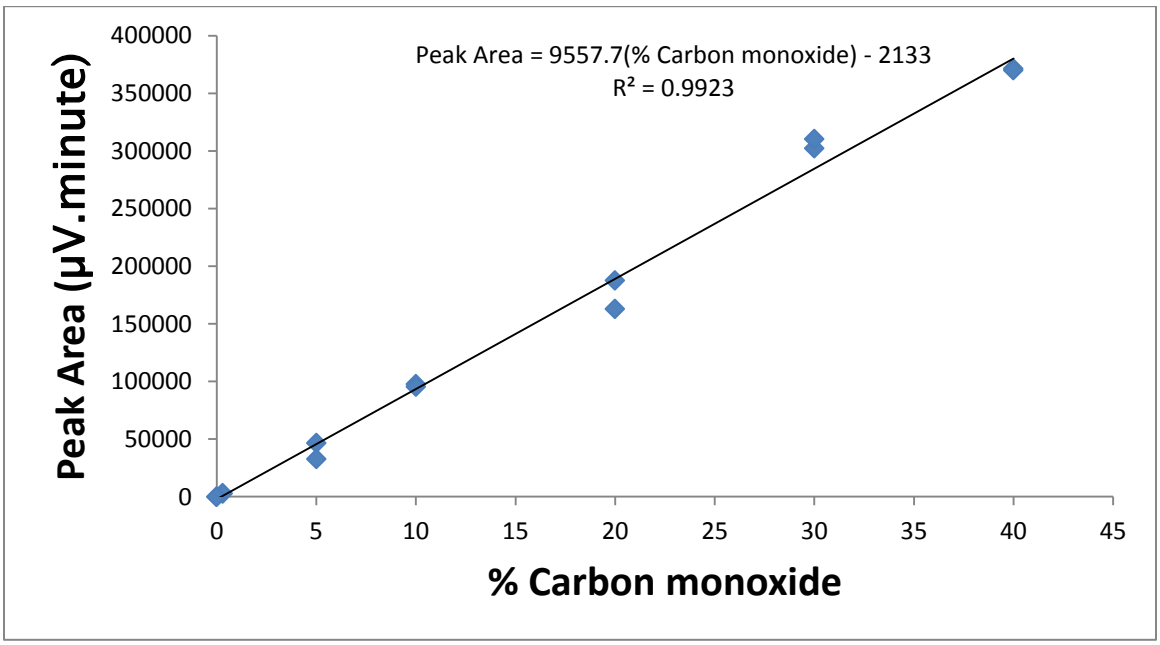

Figure 29. Calibration curve of carbon monoxide, ± 1.87% error of the value

---

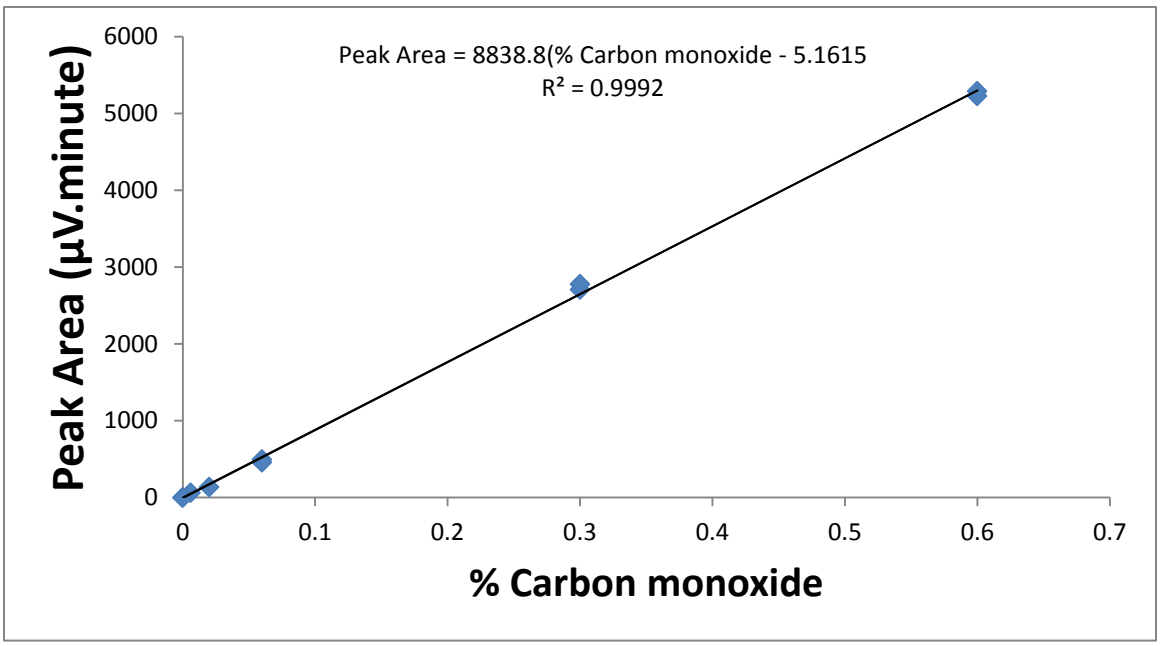

Figure 30. Calibration curve of carbon monoxide (expanded), ± 1.87% error of the value

---

The synthesis of the catalyst is divided into 5 steps

1. Pre-oxidation of graphite[53]:

   1.1 Graphite powder was added to a mixture of H_2SO_4, $K_2S_2O_8$ and P_2O_5 at 80^{O}C (Dark solution was obtained)

   1.2 The dark solution was allowed to cool down to room temperature for six hours in a standalone stirrer.

   1.3 The solution was washed with nanopure water until the pH became neutral

   1.4 The pre-oxidized graphite was dried at 35°C

2. Oxidation by graphite[54]:

   2.1 Pre-oxidized graphite oxide was added to a mixture of H_2SO_4 and $KMnO_4$ at 0°C and stirred for 10 minutes

2.2 The mixture was then stirred at 35^{O}C for 2 hours

2.3 After the two hours nanopure water was added to the mixture, and was allowed to stir for 15 minutes.

2.4 Nanopure water and 30% H_2O_2 were added to the oxidized graphite resulting in a bright yellow color shown in Figure 31.

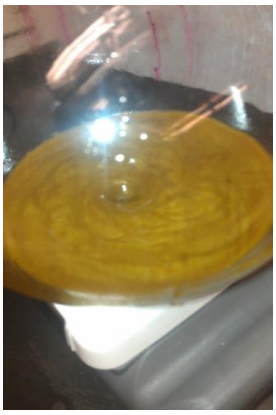

Figure 31. Oxidized graphite oxide after the addition of H_2O_2

2.5 The bright yellow solution was washed with 1:10 HCl to H_2O volume ratio

2.6 The dark brown viscous product was suspended in nanopure water

2.7 The suspended GO was washed with nanopure water to eliminate the excess HCl

2.8 Nanopure water was added to the resultant neutral GO.

3. Ionic liquid (IL) synthesis [55]:

3.1 A mixture of 3-chloropropylamine hydrochloride, 1-methylimidazole and ethanol was refluxed under nitrogen and stirrer for 24 hours at ~80^{O}C (Figure 32).

Figure 32. Ionic liquid synthesis setup

3.2 Ethyl acetate was added to the mixture resulting in a turbid mixture (Figure 33) which was dried under nitrogen at ~60^{O}C for 24 hours.

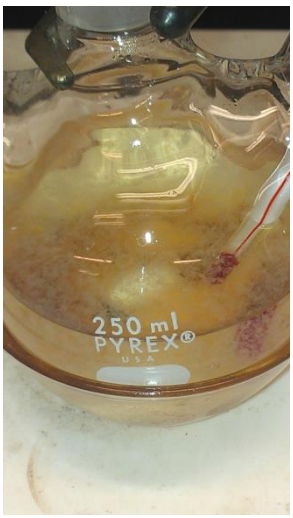

Figure 33. Ionic liquid after the addition of ethyl acetate

3.3 The resulting ionic liquid (NH_2 terminated 1-butyl-3-methylimidazolium chloride (NH_2-C_4mimCl)) is shown in Figure 34.

Figure 34. Ionic liquid

---

4. IL-reduced graphite oxide (RGO) synthesis[55]:

4.1 GO was added to the ionic liquid resulting in a brown turbid mixture shown in Figure 35.

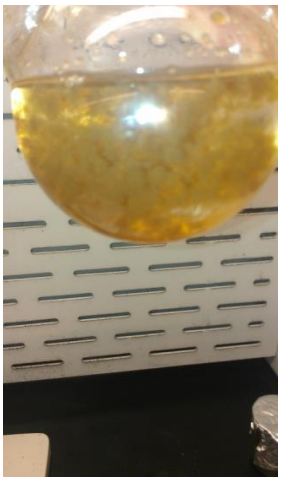

Figure 35. IL-GO

4.2 In order to allow the epoxy ring opening to occur, KOH was added to the IL-GO mixture and then it was subject to ultra-sonication for 1 hour.

4.3 During the ultra-sonication, the mixture started to change to a dark brown color due to an increase in temperature (Figure 36). The color change suggests that graphite oxide reduction was successful.

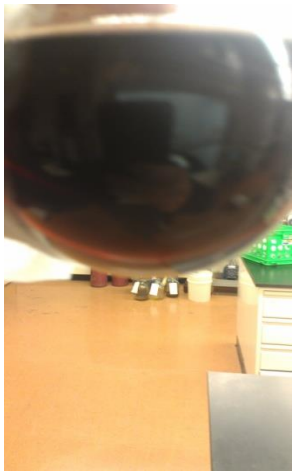

Figure 36. IL-GO after ultrasonication

4.4 The dark brown solution was stirred for 24 hours at 80^{O}C under nitrogen to have a complete reduction of the oxidized graphite (Figure 37).

Figure 37. IL-RGO

4.5 The resulting dark turbid mixture was washed with 1:10 ethanol to H_2O volume ratio.

5. IL-RGO-TiO_2 synthesis:

5.1 TiO_2 was added to a mixture of C_4mimBF_4 and H_2O[59]. The product was allowed to stir for one hour.

5.2 The washed IL-RGO was under ultra-sonication for 30 minutes.

5.3 After the ultra-sonication, the IL-RGO was added to the $TiO_2/C_4mimBF_4/H_2O$ mixture and stirred for one more hour.

5.4 The mixture was washed with a 1:10 ethanol to H_2O mixture.

5.5 The final product was dried at 80°C for 24 hours (see Figure 38).

Figure 38. IL-RGO-TiO_2

The RGO-TiO_2 catalyst was synthesized using the same procedure as the IL-RGO-TiO_2, but neither of the two ionic liquids used for the IL-RGO-TiO_2 were added.